Technical Report
TR-16-06
March 2016

Criticality effects of long-term changes in material compositions and geometry in disposal canisters

Lennart Agrenius
Kastriot Spahiu

SVENSK KÄRNBRÄNSLEHANTERING AB

SWEDISH NUCLEAR FUEL
AND WASTE MANAGEMENT CO

Box 250, SE-101 24 Stockholm
Phone +46 8 459 84 00
skb.se

SVENSK KÄRNBRÄNSLEHANTERING

ISSN 1404-0344
SKB TR-16-06
ID 1536191
March 2016

Criticality effects of long-term changes in material compositions and geometry in disposal canisters

Lennart Agrenius, Agrenius Ingenjörsbyrå

Kastriot Spahiu, Svensk Kärnbränslehantering AB

A pdf version of this document can be downloaded from www.skb.se.

© 2016 Svensk Kärnbränslehantering AB

Contents

1 Introduction

For the final repository the basic requirement concerning margin to criticality is that the effective neutron multiplication factor (k_{eff}) including uncertainties should be less than 0.95 in normal conditions. In unlikely events/accidents the k_{eff} value can exceed 0.95 but in all cases should be less than 0.98 including uncertainties.

This criterion is always fulfilled if the disposal canister is dry. If it is assumed that a canister is filled with water it is shown[1] that the criticality criterion is not fulfilled if fresh fuel without burnable poison is assumed in the canister. The criterion will, however, be met if credit for the reactivity decrease due to the burnup of the fuel is taken into account for PWR fuel and if burnable poison is credited for BWR fuel.

If water is assumed to leak in, long term chemical processes will change the material compositions and geometries in the canister during the one million year analysis period. The main process expected to affect significantly the chemical composition of the materials in the canister is the corrosion of cast iron and carbon steel of the insert, the corrosion of the stainless steel, Inconel or Zircaloy in the fuel element structural material, the corrosion of Zircaloy cladding and finally the corrosion of spent fuel itself. During metal corrosion, various anoxic corrosion products are formed, usually with lower density than the metal itself, causing thus a volume increase in the canister, accompanied by geometrical changes. In this report the reactivity effects of these changes are analyzed.

In spite of the use of massive iron canisters in almost all European repository concepts, very few studies on the influence of expanding anoxic iron corrosion products on canister criticality seem to have been carried out. We have referred to a Finnish study[2], while the study of Kienzler and Gmal (2007) was of limited use to us, given that the corrosion of iron under anoxic conditions seems to have occurred before fuel dissolution, hence oxidized iron corrosion products (hematite) and U(VI) secondary phases (schoepite) have been considered.

[1] Johansson F, Kirkegaard J, Johansson A, 2014. Kriticitetsanalys för KBS-3 systemet och slutförvaring av använt bränsle. SKBdoc 1422106, internal SKB document.

[2] Ranta-aho A, 2012. Criticality safety analysis of BWR, PWR and VVER-440 disposal canisters in the final disposal facility. TVO Memorandum 144244, internal TVO document.

2 Objective

In this study the criticality conditions are analysed in a canister taking into account changes in material compositions and geometries caused by water ingress in the long-term perspective.

The purpose is to investigate how the reactivity in the final repository is influenced by these processes as compared to the base case calculations with the initial materials[3].

[3] Johansson F, Kirkegaard J, Johansson A, 2014. Kriticitetsanalys för KBS-3 systemet och slutförvaring av använt bränsle. SKBdoc 1422106, internal SKB document.

3 Methods

All calculations were performed using Scale 5.1 with the Scale 44-group ENDF/B-V library (SCALE 2006). The code package is validated against critical experiments, see Agrenius (2010). The average value of k_{eff} for 59 calculated experiments is 0.9993 which means a bias of −0.0007Δk. The standard deviation of the 59 cases is 0.0046Δk.

It should be noted that a result from Keno V.a (normally k_{eff}) is associated with a statistical uncertainty, which has to be considered when comparing the results from two calculations. Parameters in the code have been selected so that the standard deviation of the resulting k_{eff} value is less than 0.0002.

4 Criticality safety criteria

The basic criticality criterion is that the effective neutron multiplication factor should not exceed 0.95 including uncertainties and the nuclear safety analysis should include considerations of all credible normal and abnormal operating occurrences. To meet this criterion in the canisters, credit for fuel burnup is taken for PWR-fuel and burnable absorber is credited for BWR fuel. In unlikely events, the limit is 0.98.

It is noted that criticality is achieved if $k_{eff} = 1$.

5 Description of the system

5.1 Disposal canister

Detailed descriptions of the disposal canisters are found in Agrenius (2010) and Johansson et al[4]. In summary, a disposal canister consists of an insert of cast iron with a diameter of 949 mm with a 49 mm thick outer shell of copper. The outside diameter of a disposal canister is 1050 mm. The fuel assemblies' storage positions are formed by square-formed tubes of carbon steel. The wall thicknesses of these tubes are 10 mm for the BWR-case and 12.5 mm for the PWR-case. In the BWR-insert twelve storage compartments are formed with the inner measures of 160 mm × 160 mm. In the PWR-insert four storage compartments are formed with the inner measures of 235 mm × 235 mm.

The main parameters for the canisters are shown in Table 5-1. In the calculations the values that give the highest reactivity within the tolerance limits have been used, these values are also shown in Table 5-1.

Table 5-1. Main parameters for the disposal canisters.

Parameter	BWR			PWT		
	Value	Tolerances	Used in calculations	Value	Tolerances	Used in calculations
Number of positions	12			4		
C-C distance between compartments (mm)	210	−6.4	203.6	370	−8.8	361.2
Compartment size, outer (mm)	180	± 1.8	178.2	260	± 2.6	257.6
Compartment tube wall thickness (mm)	10	± 1.0	9	12.5	± 1.25	11.25
Compartment size, inner (mm)	160		160.2	235		235.1
Insert diameter (mm)	949	+0.5/0	949	949	+0.5/0	949
Shell outer diameter (mm)	1050	+1.2/−1.0	1048.8	1050	+1.2/−1.0	1048.8
Shell thickness (mm)	49	+0.3/0	49.3	49	+0.3/0	49.3
Insert material	Nodular Cast Iron	–		Nodular Cast Iron	–	
Insert material density (kg/dm^3)	7.1	–	7.1	7.1	–	7.1
Tube material	Steel	–		Steel	–	
Tube material density (kg/dm^3)	7.85	–	7.85	7.85	–	7.85
Insert lid material	Steel			Steel		
Insert lid material density (kg/dm^3)	7.85		7.85	7.85		7.85
Shell material	Cu	–		Cu	–	
Copper density (kg/dm^3)	8.9	–	8.9	8.9	–	8.9
Length of compartment (mm)	4463	+5/−10	4448	4443	+5/−10	4448
Length of insert (mm)	4573	0		4573	0	
Length of canister (incl. Cu shell)	4835	+3.25/−2.75	4672.25	4835	+3.25/−2.75	4672.25

[4] Johansson F, Kirkegaard J, Johansson A, 2014. Kriticitetsanalys för KBS-3 systemet och slutförvaring av använt bränsle. SKBdoc 1422106, internal SKB document.

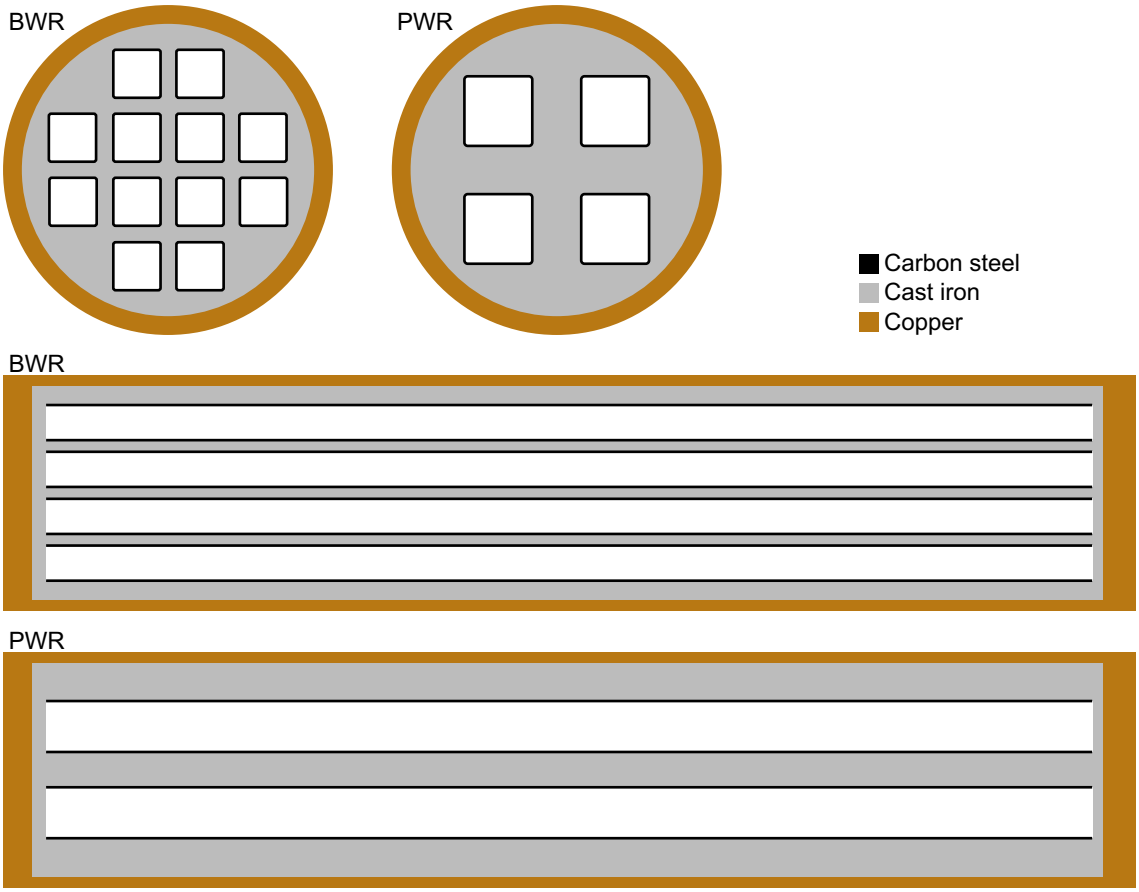

Figure 5-1. *Cross sections of the BWR- and PWR-disposal canister.*

5.2 Fuel types

In the current criticality analysis for the KBS-3 system and final repository of spent nuclear fuel[5] the most reactive fuel types are identified. It is shown that the most reactive fuel assembly type in disposal canister geometry is W15x15UPGRADE for PWR and SVEA 96 Optima 3 for BWR. As shown in the reference, these fuel types cover all different fuel types including MOX-fuel and will be used as reference fuel types in this study.

In the calculations 5 % U-235 enrichment is assumed for PWR. For BWR 3.2 % enrichment is used. This is the enrichment corresponding to a 5 % U-235 enriched fuel with credit for burnable poison[6], at least 14 fuel rods with 5.5 % Gd_2O_3.

[5] Johansson F, Kirkegaard J, Johansson A, 2014. Kriticitetsanalys för KBS-3 systemet och slutförvaring av använt bränsle. SKBdoc 1422106, internal SKB document.

[6] Johansson F, 2015. Kreditering av BA i BWR bränsle. SKBdoc 149344, internal SKB document.

6 Analysis

6.1 Introduction

When loaded in the final repository the canisters are dry and filled with argon. The k_{eff} in this condition is shown below:

Dry canister

PWR: $k_{eff} \pm \sigma = 0.2900 \pm 0.0002$

BWR: $k_{eff} \pm \sigma = 0.2322 \pm 0.0002$

The k_{eff} is then calculated for BWR and PWR, assuming that the canisters are filled with water and the geometries of the canister and the fuel are intact. In order to be able to model the growth of corrosion products in the canister channels walls, the fuel assemblies were assumed here located in the center of their respective channels, in contrast to the criticality analysis for the KBS-3 system and final repository of spent nuclear fuel[7], where the assemblies were placed eccentrically.

Water filled canister

PWR: $k_{eff} \pm \sigma = 1.0993 \pm 0.0002$

BWR: $k_{eff} \pm \sigma = 0.9142 \pm 0.0002$

In the criticality analysis for the KBS-3 system and final repository of spent nuclear fuel[8] it is shown that k_{eff} is less than 0.95 if the average fuel assembly burnup is higher than 34 MWd/kgU for PWR assuming that both actinides and fission products are taken into account.

6.2 Water ingress

To get water into a canister it is assumed that a breach is formed in the copper shell through which water will flow into the canister. The scenarios leading to a water filled canister in repository's long term evolution are those discussed in the SKB's most recent safety assessment, SR-Site (SKB 2011). The risk contributing scenarios discussed in SR-Site are: a) canister failure due to shear load (in case of a large earthquake in the vicinity of the repository) and b) canister failure due to corrosion (for advective conditions in the bentonite buffer, assumed to be caused by buffer erosion).

The calculated mean number of failed canisters due to a large earthquake in the vicinity of the repository at the end of the 1 000 000 year assessment period is 0.079 (SKB 2011). After the canister shear, it takes a relatively short time (assumed to be 100 years) to have the canister filled with water and the insert and all the metallic parts in the fuel element begin to corrode (SKB 2010b, SKB 2011).

The estimated times of canister failure due to bentonite erosion and subsequent enhanced copper corrosion due to sulphide are of the order of 100 000 years. This type of failure is assessed to occur only if the few canisters exposed to the most severe flow conditions are also exposed to the highest groundwater sulphide concentrations observed at the site, whereas the overwhelming majority of the canisters are calculated to withstand this failure mode with a margin at the end of the 1 000 000 year assessment period. In this case when the penetration of water occurs, the copper shell has a relatively large damage and thereafter the canister is filled with water. At this point, the corrosion of the insert and other metallic parts in the fuel elements starts, as well as fuel dissolution. It should be noted that during such long time periods, changes in the fuel composition due to radioactive decay have

[7, 8] Johansson F, Kirkegaard J, Johansson A, 2014. Kriticitetsanalys för KBS-3 systemet och slutförvaring av använt bränsle. SKBdoc 1422106, internal SKB document.

to be considered, for example most of the ^{239}Pu has decayed to ^{235}U. Such changes in composition are accounted for in the calculations of fuel reactivity change as a function of time, presented for example in Figure 33 and Figure 34 of Agrenius (2010).

6.3 Long term evolution of a breached canister.

Directly after water contact, simultaneous corrosion of several materials starts and with time will cause changes in the geometry (metals will be consumed and corrosion products with higher molar volume will be produced) and in the material composition of all canister components. This is a very complex process which depends on a multitude of parameters, and different geometrical configurations are obtained e.g. if the Zircaloy cladding is completely corroded before or after the filling of the internal free space in the canister with corrosion products. For this reason here it will be attempted first to evaluate the most probable evolution of the system, i.e. the main evolution case, striving to use realistic corrosion rates for all components under the given conditions and not e.g. conservative upper values to cover for uncertainties, as may be done when release of activation products has to be estimated. All conceivable configurations that can be derived from the range of possible corrosion rates for all materials can then be analysed systematically by judging the consequences of a different corrosion rate for a given component. Note that in this report, the term "scenario" is not used in its usual meaning in safety analysis (see for example Section S 3.9 in SKB 2011), rather as a synonym for "case" in certain occasions. Thus for example, cast iron corrosion rates of 1 μm/ year are chosen for the base case, while higher corrosion rates, for example 10 μm/year, are also possible, but, as it will be shown later here, they would just shorten the time to realise the cases analysed here and would not add new cases. This alternative was preferred to the study of all cases obtained by a random combination of corrosion rates within a given interval for all the different materials. During this analysis, special care was devoted to parameter ranges which give rise to scenarios resulting in increased reactivity. Thus for example, high Zircaloy corrosion rates give rise to scenarios with fuel pellets at the bottom of the fuel channel, which (as it will be shown in Section 6.4.8) result in a reactivity decrease. For this reason, calculation cases based on relatively low corrosion rates for Zircaloy were analysed in more detail.

The approach followed here is also to evaluate all conceivable configurations in the canister, while the time at which they are achieved is less important from the reactivity point of view, if all calculations are made with the fuel having the highest reactivity over time. As mentioned before, the reactivity of the spent nuclear fuel varies with time during the 1 million year period analysed. In order to avoid dependence on this parameter, all calculations are carried out with the highest reactivity of the fuel over time. Further, pure water has been used conservatively in all the calculations, instead of groundwater.

Given the complex system under investigation, the reasoning followed here for the less probable system evolutions has been to evaluate their consequences for material configurations which result in increased reactivity. Thus, for example the analysis of the main evolution case assumes in general a long life to the cladding tubes. However, a case when the corrosion of for example Zircaloy has, for some reason, been faster than what is assumed in the main case, leading to a configuration with fuel pellets at the bottom of the fuel channel is also included. The consequences of this case have been evaluated for a magnetite layer that has grown until almost touching the fuel rods.

There are several parameters and properties for which there are no published data, or which are difficult to evaluate due to the extremely large time span of the analysis. In this category fall for example the properties of hydrated magnetite, which is indicated as the main corrosion product of carbon steel and cast iron by most of the experimental studies. In our case we have evaluated the properties of hydrated magnetite, including its density, by using homogeneous mixtures of crystalline magnetite and water. This is expected to be an adequate representation of the position of the nuclei and their interactions with the neutrons in hydrated magnetite, when there are no data in the literature even for the density of this material.

In the following, the long term corrosion of carbon steel and cast iron will be discussed first, then the corrosion of metallic parts of the fuel elements and of the zircaloy cladding, always from the point of view of potential material redistribution and geometry changes in the damaged canister.

6.3.1 Long-term corrosion of cast iron and carbon steel

The corrosion of cast iron under the anoxic conditions expected to prevail in the canister is expected to produce mainly magnetite and hydrogen, according to:

$$3Fe(s) + 4H_2O(l) = Fe_3O_4(s) + 4H_2(g) \quad (6\text{-}1)$$

The long-term corrosion rate under anoxic conditions is also independent of whether or not water is present as liquid or as vapour (Smart et al. 2002b), thus we have assumed the whole surface of cast iron insert, including the carbon steel at the fuel channels, to corrode at constant rate. Several experimental studies have shown the absence of localized corrosion in these materials under repository conditions (SKB 2010a), hence uniform corrosion is assumed to take place during the whole time interval analysed. This means that the thickness of the corroded layer is assumed equal for all surfaces of cast iron or carbon steel in contact with water.

The corrosion product magnetite is reported to consist of two layers: a thin, strongly adherent layer and an outer layer of poor adhesion (Smart et al. 2002b). According to these authors, the adherent layer is formed directly on the surface of the metal by reaction (6-1), while the looser layer is probably formed by the precipitation of dissolved Fe(II) ions. The adherent layer forms very quickly and then does not increase further in thickness, while continuing corrosion leads to the thickening of the non-protective layer. The corrosion rate is controlled by ion transport through the adherent layer and is expected to continue at constant rate over long periods of time.

The density of magnetite is lower than that of the metal, meaning that corrosion of the cast iron insert will be accompanied by a volume increase. The density of crystalline magnetite (formed for example by high temperature iron oxidation) is reported in literature as 5.17 g/cm^3 (Haynes et al. 2012), and in mineralogical databases as 5.15 g/cm^3, the average of magnetite densities in the interval 5.1–5.2 g/cm^3 (Mineralogy database 2012). The volume increase of magnetite in comparison to the volume of cast iron used to produce this quantity of magnetite, or the Pilling-Bedworth ratio (P-B ratio) (Pilling and Bedworth 1923), is:

$$R_{PB} = \frac{V_{oxide}}{V_{metal}} = \frac{M_{oxide} \cdot \rho_{metal}}{n \cdot M_{metal} \cdot \rho_{oxide}} = \frac{231.53 \cdot 7.85}{3 \cdot 55.845 \cdot 5.17} = 2.10$$

where V denotes molar volume, M denotes molar or atomic mass, ρ denotes density and n is the number of metal atoms per molecule of the oxide.The R_{PB} values for other potential corrosion products formed under reducing conditions as for example $Fe(OH)_2$ are higher, of the order of ~ 3.7, hence a volume increase of the corrosion products as compared to the corresponding volume of corroded cast iron of 2–4 times has to be expected. The same holds for other potential corrosion products which may form under reducing conditions, such as green rust or siderite. As mentioned above, most of the magnetite produced in the non-protective layer is very probably a hydrated form of magnetite, less compact than crystalline magnetite.

A large effort has been devoted in the past to investigate the potential mechanical damage of the copper canister due to the volume increase of iron corrosion products formed by the corrosion of cast iron in the space between copper and iron (Bond et al. 1997, Winsley 2008). As discussed in a literature review on the mechanical properties of iron oxides (Winsley 2008), the only experimental measurements of the mechanical properties of the magnetite formed during anoxic corrosion of cast iron in groundwater at low temperatures are those of Smart et al. (2001, 2006a). The mechanical properties of a magnetite film grown on the surface of cast iron and carbon steel coupons in two artificial groundwaters of pH 7–8 or pH 10.4 at 50 or 80 °C were studied by AFM (Atomic Force Microscopy) and a nano-indentation technique. The Young's modulus values for anaerobically formed low temperature magnetite were in the range 4×10^4 to 2×10^6 Pa. These values are several orders of magnitude lower than for bulk magnetite or magnetite films formed at high temperature.

Evidence for the fact that the expansion effects due to the formation of anoxic corrosion products on cast iron are expected to be relatively small comes from experimental studies and archaeological observations.

Experimental studies have been carried out to measure directly the expansion caused by the anaerobic corrosion products of carbon steel and cast iron in a simulated repository environment whilst under representative compressive loads (Smart et al. 2006a). The apparatus consisted of a

stack of 100 alternate copper and ferrous washers, which were corroded anaerobically in artificial groundwater at 69 °C. Changes in the height of the stack were amplified and could be measured by a displacement transducer. The amplification was such that a change of 1 nm thickness of the corrosion layer in each of the 200 corroding interfaces could be detected. No displacement of the stack was detected for applied loads of 1 MPa and 10 MPa, because the corrosion product formed was probably easily compressed or extruded from the space between the discs. That corrosion took place, was indicated both by hydrogen production and the analysis of magnetite in the corrosion products.

A study of the corrosion of the Coppergate helmet (Tweddle 1992), buried for more than 1200 years, shows that the anaerobic corrosion product (siderite in this case) does not cause expansive damage even in tight crevices such as those under rivet heads or iron cap sheets of the Coppergate helmet or between copper sheet and iron in Iron Age artefacts (Smart and Adams 2006).

The mechanical properties of the corrosion product magnetite formed at low temperature are due to its higher proportion of water (Smart et al. 2006a), in contrast to the situation in concrete, where the supply of water is limited, or the oxide films formed at high temperature, which have a much higher hardness and lower water content. According to Smart et al. (2006a) "If water were to penetrate the outer canister wall and enter the annulus, it is likely that any anoxic corrosion product formed would deform and spread around the annulus, rather than expand to force the copper outer canister away from the iron insert. Eventually the annulus may fill up with corrosion product, which would gradually be compressed by the confining walls of the canister. Subsequent corrosion would depend on whether water could penetrate the corrosion product in the annulus and reach the surface of the iron insert".

In this report we have used the hypothesis based on the results of Smart et al. (2006a) that the magnetite formed in the region between copper and cast iron will extrude in the free space in the canister, instead of causing a deformation of the copper shell. Even in other cases, when magnetite is formed in confined spaces as for example between the fuel channels and the zircalloy fuel box, it has been assumed as more probable that the magnetite with extrude and fill the available free space, causing no or only a limited deformation of the fuel box. In general, in such cases an indicative calculation of the reactivity of the system is done even for the less probable case, i.e. also for a case when the formed magnetite deforms the copper shell or the fuel box (reduced fuel pitch, Section 6.4.4).

Another issue which is difficult to verify is the distribution of the corrosion products during time spans of tenths or hundreds of thousand years, for which no experimental or archaeological data exist. Thus, the geometry of the damaged canister would be different if the formed magnetite stays at the place where it is formed, even when it reaches several centimetres of thickness, or falls down in the fuel channel. In this case we have used expert judgement, by consulting three corrosion experts (D. Shoesmith, N. Smart, F. King) in order to choose the most probable evolution, i.e. with the magnetite layer continuing to grow on the cast iron surface and not fall down. However, a calculation for the other variant has also been carried out, see further in next section.

The corrosion rate of cast iron and carbon steel in a damaged canister under repository conditions is one of the most important parameters in evaluating the future evolution of the canister interior. In SR-Site, the corrosion rate of cast iron is based on the experimental studies by Smart et al. (2002a, b) in synthetic groundwater. The corrosion rate has proven to be independent of both hydrogen gas pressure and Fe(II) concentration in solution. The long-term corrosion rate is independent of whether or not the water is as a liquid or as vapour. The mean corrosion rates were low and generally less than 1 μm/year. The measured rates span nearly two orders of magnitude, although most data indicate a rate of less than 0.1 μm/year (SKB 2010a).

In another series of studies of cast iron corrosion under anoxic conditions in the presence of bentonite clay, slightly higher corrosion rates were observed (Smart et al. 2004a, 2006b, 2008), as well as adsorption of large quantities of iron ions in the bentonite. Most of the corrosion rates measured in the presence of the bentonite was of the order of 1–2 μm/year after one year, even though a decrease of the corrosion rate with time is always observed also in these tests.

A large number of archaeological objects corroded under anoxic conditions has been analysed with different methods, both by SKB (Smart and Adams 2006) and by others (Neff et al. 2006, Saheb et al. 2008, 2010, 2012). The corrosion rates for iron objects corroded under anoxic or reducing conditions are in the range 0.1–2 μm/ year. In many of these objects, thick corrosion layers are observed and in many cases concretion is commonly formed around iron objects, by iron corrosion

products mixing with material adjacent to the iron. It is predominantly composed of $CaCO_3$, which undergoes ion exchange with the iron ions released by corrosion to form $FeCO_3$ and other iron compounds. The structure of the concretion is different depending on whether it is exposed to seawater or buried in sediment. In buried conditions the concretion contains predominantly Fe_3O_4, compared to FeOOH and Fe_2O_3 in exposed to air situations. It seems highly probable that thick layers of corrosion products can be formed on the surface of the cast iron. As discussed in Saheb et al. (2012), the corrosion rates estimated for 500 year old archaeological objects are of the same order of magnitude (0.6–2 μm/year) as for short term corrosion experiments, suggesting that the presence of the thick corrosion layer does not influence significantly the process.

Based on several reviews of carbon steel and cast iron corrosion under repository conditions (Gribi et al. 2008, King 2008, 2014, Andra 2005, Féron et al. 2009), as well as the data of Smart et al. in the presence of bentonite (Smart et al. 2004a, 2006b, 2008) and the archaeological studies mentioned above, a corrosion rate of 1 μm/year seems as the most reasonable choice for discussing the main evolution case of a damaged canister. However, the consequences of a lower corrosion rate, e.g. of the order of 0.1 μm/year, will be considered in calculation cases with such rates. Given that 0.1 μm/year is the lowest limit of corrosion rate range reported in archaeological studies, corrosion rates lower than this value for cast iron have not been considered. In this report, we are more interested in the potential configurations of all the materials during the long term evolution of a damaged canister and a higher corrosion rate for cast iron simply means that a given situation occurs proportionally earlier then when considering for example a ten time lower corrosion rate. This is why higher corrosion rates, for example 10 μm/year, even though possible, are not analysed here-they would not bring any new configurations as compared to the ones analysed.

6.3.2 Potential formation of other anoxic corrosion products

As discussed above, magnetite is the most probable corrosion product, based on evidence from experimental and archaeological studies. However, other anoxic corrosion products have also been observed under different experimental conditions or are found in various archaeological objects. In corrosion studies carried out in media containing higher carbonate concentrations (e.g. Legrand et al. 2000, Savoye et al. 2001) and in archaeological objects especially those found in clay environments where the carbonate concentration is also relatively high (for example the Coppergate helmet discussed above in Smart et al. 2006a), siderite (iron(II) carbonate) is found as corrosion product. In Table 6-1, the phases formed during a few experimental studies of iron corrosion carried out in solutions containing various levels of carbonate are summarised.

Table 6-1. Iron corrosion products observed in experimental studies with carbonate containing solutions.

Iron form	Solution composition	Corrosion products observed	Reference
Carbon steel	*Deaerated solutions:*		(Refait et al. 2012)
	0.003 M $NaHCO_3$	Green rust carbonate, magnetite	
	0.1 M $NaHCO_3$	Green rust carbonate	
	1 M $NaHCO_3$	Siderite	
	0.003 M $NaHCO_3$ + 0.3 M Na_2SO_4	Green rust sulphate, green rust carbonate.	
	0.03 M $NaHCO_3$+ 0.03 M Na_2SO_4	Green rust carbonate, chukanovite	
Pure Fe powder	Distilled water + Callovo-Oxfordian clay, de-aerated solutions, T = 90 C	Magnetite, iron rich silicates (greenalite or cronstedtite) or chlorite.	(de Combarieu et al. 2007)
Fe powder (99 %)	Synthetic groundwater, anaerobic conditions	Iron(II) hydroxide, later transformed to magnetite	(Odziemkowski et al. 1998).
Carbon steel	*Anoxic solutions:*		(Lee et al. 2006)
	1 M Na_2CO_3/$NaHCO_3$	Siderite	
	0.2 M Na_2CO_3 / $NaHCO_3$ + 0.1 M Na_2SO_4	Siderite, magnetite, green rust carbonate, green rust sulphate.	
	0.2 M Na_2CO_3 / $NaHCO_3$ + 0.1 M Na_2SO_4 + 0.1M NaCl	Green rust carbonate, magnetite, siderite, green rust sulphate.	
	0.2 M Na_2CO_3 / $NaHCO_3$ + 0.1 M Na_2SO_4 + 3 M NaCl	Green rust carbonate, siderite.	

Siderite, $FeCO_3(s)$ is usually formed in groundwaters with relatively high carbonate concentrations (see Table 6-1) through the reaction:

$$Fe(s) + HCO_3^- + H^+ = FeCO_3(s) + H_2$$

In addition, green rust type phases (double layer mixed Fe(II)/Fe(III) hydroxides) may form, but they are metastable with respect to magnetite and siderite.

At relatively high concentrations of sulphide, various forms of iron(II) sulphide compounds may form as corrosion products:

$$Fe(s) + HS^- + H^+ = FeS(s) + H_2$$

In an experimental study of the corrosion of carbon steel by aqueous hydrogen sulphide at low temperatures (Shoesmith et al. 1980), the formation of up to three iron monosulphide phases is reported: mackinawite (tetragonal $Fe_{1+x}S$), cubic ferrous sulphide and troilite (stoichiometric hexagonal FeS). At pH over 6, only mackinawite was formed as corrosion product and will be discussed further here. The concentrations of sulphide in Forsmark are in the interval 10^{-4} to 10^{-6} M, i.e. relatively low to cause substantial sulphide corrosion. Because of the large defect in both analysed scenarios, large amounts of hydrogen are expected to be produced in the damaged canister and, especially in the erosion/corrosion case, the possibility of microbial reduction of sulphate by SRB (Sulphate Reducing Bacteria) using the hydrogen is a possibility. The utilisation of hydrogen by SRB was considered as the cause of the fast iron corrosion, but this hypothesis has been questioned lately (Enning et al. 2012, Enning and Garrelfs 2014). In 2004 experimental evidence was presented for a novel corrosion mechanism, in which microbial reduction of sulphate was carried out through direct consumption of iron derived electrons through the semiconducting sulphide layer, without involving hydrogen as an intermediary (Dinh et al. 2004). Without going into details, we point out the following: Chemical microbially influenced corrosion (CMIC) of iron by hydrogen sulphide from microbial sulphate reduction occurs with "natural" organic substrates. There are certain SRB strains which corrode iron by direct utilisation of the metal itself, through a direct electron uptake in the microbe (EMIC). Further, different corrosion products are formed by CMIC (only sulphide) and EMIC, a mixture of iron carbonate (siderite) and sulphides (ca. 25 %, mainly mackinawite). The corrosion rates involving microbial corrosion are usually high.

In any case, even by assuming an average concentration of sulphate of 5 mM for the groundwaters in Forsmark during the whole 1 million year analysis period, around 1.5 moles of sulphide per canister and year can be produced by assuming complete microbial reduction of all sulphate. This means that mass balance calculations allow calculating a maximum of iron sulphide that can be present as corrosion product in the canister, where magnetite will anyhow dominate (see Appendix B). In this estimation, any consumption of sulphide by copper (highly probable) has been neglected. At the same time, enough reductant (for example H_2 produced by iron corrosion) has been assumed to be available for the microbes to convert 1.5 moles of sulphate into sulphide (about 6 moles H_2/year).

The formation of siderite with the predicted carbonate concentrations during Forsmark groundwater evolution seems also less probable; a potential pathway may anyhow be through EMIC corrosion or through concretions formed by interaction of magnetite with groundwater. Further, the maximum amount of siderite than can be formed during the corrosion of the cast iron insert of a KBS-3 canister may be estimated by the average carbonate/bicarbonate concentration in the groundwater and an assumed high flow through the canister. The carbonate concentrations in Forsmark are expected to vary during the 1 000 000 year analysis period between 0.23 mM to 6 mM, depending on the climate conditions (Salas et al. 2010, Joyce et al. 2015). Assuming an average total carbonate concentration of 6 mM in the groundwater during the whole period and a groundwater flow of 300 l/year through the deposition hole, a maximum of 1.8 moles of carbonate per canister and year can be produced. The amount of the siderite in the siderite-magnetite mixtures is estimated following two different assumptions, see Appendix B.

To investigate the influence of such corrosion products in the canister reactivity, calculation cases by assuming partial formation of mackinawite or siderite as corrosion products have been carried out. We have carried out the calculations with siderite and mackinawite for the corrosion product configuration which results in high reactivity, i.e. when the corrosion layer approaches the fuel rods. For siderite, using a theoretical density of 3.87 g/cm^3, the Pilling-Bedworth ratio is 4.2, i.e.

when a carbon steel layer of 3.15 mm has corroded, the corrosion layer just touches the fuel rods. The volume of iron needed to corrode in order to produce 1 m^3 of siderite is 1/4.2 = 0.238 m^3 and the situation of a completely filled space in the canister may be achieved about twice as quickly as when the corrosion product is magnetite.

There are several iron sulphide phases which may form during iron corrosion in the presence of high sulphide concentrations. Experimental studies (Shoesmith et al. 1980), as well as archaeological studies report formation of mackinawite ($Fe_{1+x}S$, x = 0-0.1) under the experimental conditions similar to the ones expected in the repository. By using a density of 4.3 g/cm^3 and a molecular weight of 84.7 g/mol, the Pilling-Bedworth ratio for crystalline mackinawite is 2.76. From this, the layer of iron which is corroded when mackinawite touches fuel rods and the volume of iron needed to be corroded to fill a BWR or PWR canister with mackinawite can be estimated.

Based on the above discussion, four calculation cases are considered with the corrosion layer being a mixture of magnetite with mackinawite in two cases and magnetite with siderite in the two other cases for both BWR and PWR canisters. The configuration of the corrosion product assumed for these calculation cases corresponds to the one which results in an increased reactivity, see next section (Section 6.4.2) for a discussion of calculation cases.

6.3.3 Corrosion of zircalloy and stainless steel

As mentioned before, at the same time as the canister is filled with water and the corrosion of cast iron starts, the corrosion of Zircalloy cladding tubes as well as the corrosion of spacer grid plates, top and bottom plates and other metallic parts in a fuel elements starts.

The corrosion of Zircaloy at relatively low temperature (20–80 °C) proceeds at such low rates that it is impractical to conduct meaningful corrosion test under any reasonable time period (IAEA 1998). Zircaloy coupons were exposed in two Hanford fuel storage pools for a period of three years, during which water chemistry changes occurred which markedly accelerated corrosion of Al alloy and carbon steel specimens. The Zircaloy specimens maintained their silver appearance and the oxide growth was less than the first interference colour range (20 nm thickness), indicating a corrosion rate less than 7 nm/year (Johnson and Burke 1996). This is why corrosion rate correlations generated at high temperature are used to make estimations for corrosion rates at the lower temperatures, such as those expected under repository conditions. Table 20 in Gras (2014) summarizes the metal loss rates predicted from 10 corrosion models of Zircaloy derived from high temperature data and published from 1964 to 1998. When these models are used to extrapolate corrosion rates to 20 and 50 °C, values between 10^{-11} and 10^{-4} nm/year are obtained, supporting the statement that it is very difficult to measure such rates experimentally. As discussed in Shoesmith and Zagidulin (2011), despite the presence of radiation fields associated with the fuel, the redox conditions within a waste canister will remain reducing due to the production of oxidant scavengers Fe(II) and H_2 by iron corrosion. Consequently, the only feasible corrosion mode that could lead to degradation of the cladding is passive corrosion. A corrosion rate of 5 nm/year is considered as base case for estimating activation product releases. As discussed before, the lower corrosion rate interval is more interesting for this study. The corrosion rates of Zircaloy in granitic groundwaters at temperatures around 20 °C are very likely to be as low as 1–2 nm/year (Gras 2014, Shoesmith and Zagidulin 2011, SKB 2010a).

In spite of the limited thickness of the Zircaloy cladding (less than a millimetre), it is expected to have enough un-corroded metal for time intervals of the order of a few tens of thousands of years to assure their mechanical stability until all the free space in the canister is filled with magnetite. With a corrosion rate of 1 µm/year and 33 m^2 of internal cast iron surface in a canister (SKB 2010a), the time needed to corrode 0.474 m^3 cast iron, which gives 1 m^3 of crystalline magnetite is less than 15 000 years. Of course, in case hydrated magnetite, which is less dense, or any other anoxic corrosion product as for example $Fe(OH)_2(s)$ is produced, this time will be shorter. To bound from the other side, when the corrosion of cast iron proceeds with 0.1 µm/year, the free space inside the canister will be filled with magnetite for time intervals of the order 150 000 years. Even at such time spans, the Zircaloy cladding will not be corroded completely, if Zircaloy corrosion rates are of the order of 1–2 nm/year. In any case, a calculation case with higher corrosion rate for the Zircaloy cladding resulting in its complete corrosion and the fuel pellets at the bottom of the fuel channels has also been carried out. As can be seen in next section, this case results in lower reactivity as compared to the case when the fuel pellets remain inside the Zircaloy cladding, hence no further analysis of consequences of higher Zircaloy corrosion rates has been undertaken here.

Corrosion of stainless steel and Inconel in structural parts of fuel element is expected to occur more slowly, probably at 10 to 100 times lower rates than that of the cast iron under the same conditions, based on several literature data discussed for example in SKB (2010a). The potential for localized corrosion under the anoxic and reducing condition expected in the repository is relatively small as discussed in SKB (2010a), based among others on the data of Kursten et al. (2004). Under anoxic conditions (Wada et al. 1999) measured very low corrosion rates (< 0.01 μm/year) of 304 SS stainless steel, the material of the hull-end pieces of the fuel elements, in seawater based groundwater of pH 10. Smart et al. (2004b) report anaerobic corrosion rates of stainless steel in alkaline environments in the range of 0.01 to 0.1 μm/y. The corrosion rates under anoxic conditions in alkaline environments were found to be relatively insensitive to pH within the range 6.4 to 13 (Blackwood et al. 2002).

A specific case in the fuel elements are the grid spacers, made of Zircaloy or Inconel, which are usually thinner than the other parts and may be consumed faster, especially in the case of Inconel. The corrosion of grid spacers could affect the geometry of the fuel rods in a fuel element. Anyhow, the effect is expected to be limited, because the top and bottom plates are much thicker and they are not expected to have corroded significantly during the few tens of thousands of years it takes to fill the space between the fuel rods with magnetite. A special case here are the BWR fuel elements, which may contain up to 14 partial length rods, which are not attached to the top plate. Another special case are some BWR assembly types that have no top plate. Calculation cases for these situations have been carried out, see Section 6.4.7.

6.3.4 Corrosion of spent fuel

As soon as the canister is filled with water, the corrosion of the spent fuel also starts. In the first period, the release of the IRF (Instant Release Fraction) occurs, consisting in the release of a few percent of the inventory of volatile fission products such as Cs and I. Under the reducing conditions created by the anoxic corrosion of iron, the dissolution rate of spent fuel matrix is expected to occur with an average rate of 10^{-7}/year (SKB 2011, 2010a, b). This corresponds to an amount of around 3 kg U dissolved during for example 15 000 years needed to fill the canister void with iron corrosion products. As discussed in SR-Site (SKB 2011), this oxidized uranium is expected to be reduced and precipitated as secondary UO_2(s) on the surface of the corroding cast iron. Evidence for the reduction of oxidized U(VI) on the surface of corroding iron is ubiquitous, both from experimental studies related to geological disposal (Grambow et al. 1996, Cui and Spahiu 2002) and in studies of removal of uranium using zero-valent iron (Fiedor et al. 1998, Gu et al. 1998, Farrell et al.1999). In solution only a small amount of uranium, corresponding to the low solubility of UO_2(s) under reducing conditions (3×10^{-9} M or 7.5×10^{-7} g/l), is expected to be found. Given that preliminary calculations indicated a slight increase in reactivity due to this redistribution of uranium, the amount of uranium dissolved and deposited on the magnetite layer was estimated for the lower corrosion rate of cast iron (0.1 μm/year), resulting in longer time periods (90 000 years to corrode 9 mm steel) and larger quantities of redistributed uranium (18 kg in this case). The dissolution of the fuel matrix is assumed to occur congruently, i.e. the fission products (such as lanthanides) and the actinides (such as e.g. Pu), which are distributed homogeneously in the matrix, are released together with U. This means that 18 kg of fuel material including U, Pu, fission products and other actinides are released and expected to co-precipitate together with U on the surface of corroding iron. In another calculation case, only U and Pu are assumed to be reduced and precipitated on the surface of the corroding iron. Calculations to consider these effects have been carried out, see Section 6.4.9.

6.4 Evolution in time of a damaged canister

6.4.1 Main evolution scenario

Calculations show that the substitution of cast iron or carbon steel with magnetite is accompanied with an increase of the reactivity in the damaged canister, see Table 6-2. In this hypothetical calculation, the whole volume occupied by carbon steel and cast iron in the canister was assumed to be substituted by crystalline magnetite.

Table 6-2. k_{eff} in canister with different material in insert (σ = ± 0.0002).

	Insert material	
Fuel type	**Cast iron**	**Magnetite**
PWR	1.0993	1.1039
BWR	0.9142	0.9266

As discussed above, the corrosion will take place on surfaces that are exposed to water. The growth of magnetite will decrease the gap between the channel wall and fuel rods. The reactivity effect of this is shown in Figure 6-1 for PWR.

It can be seen that maximum reactivity (k_{eff} = 1.1159) occurs when the layer of magnetite has grown and the gap between the magnetite and the fuel rod surface is around 2 mm. The space in-between the fuel rods and the gap is still water filled. This corresponds to the corrosion of a carbon steel layer of about 9 mm (this would give a 19 mm corrosion layer thickness assuming the density of crystalline magnetite and thicker layer if hydrated magnetite or other anoxic corrosion products are formed). The assumption made here is that the magnetite formed does not fall down in the fuel channel, but remains in the walls, as discussed before. Given the large defects in the copper shell in both the shear load scenario and erosion/corrosion scenario, the presence of a sufficient quantity of water to cause corrosion has been assumed here. Continued growth of the magnetite layer will result in reactivity decrease when the magnetite layer continues growing into the fuel assembly between the fuel rods (this is represented in Figure 6-1 with negative values for the gap size).

These calculations were also done for the BWR-case. Note that BWR-fuel bundle is placed in a fuel box and magnetite layer will grow against this box wall.

It can be seen in Figure 6-2 that maximum reactivity (k_{eff} = 0.9475) occurs when the layer of magnetite has grown and the gap between the magnetite and the box wall is closed. This case also corresponds to the corrosion of a carbon steel layer of about 9 mm which gives a 19 mm corrosion layer thickness. It should be mentioned that the carbon steel of the fuel channels contains maximum 0.22 % carbon, mainly in the form iron of carbides, while cast iron contains ~ 4 % C, mainly as graphite. The iron carbides react with water to produce iron oxides plus different forms of organic or inorganic (i.e. carbonate) compounds, either gaseous or soluble in water (Swanton et al. 2015), usually at slower rates than the steel itself. We have carried out a calculation of the case described here with the gap between fuel channel and the fuel rods filled with magnetite including 0.22 % C in the magnetite composition, i.e. neglecting any reaction of the iron carbides with water. A reactivity increase of Δk_{eff} = 0.0004 was obtained for the BWR case, while in the PWR case the increase was negligible.

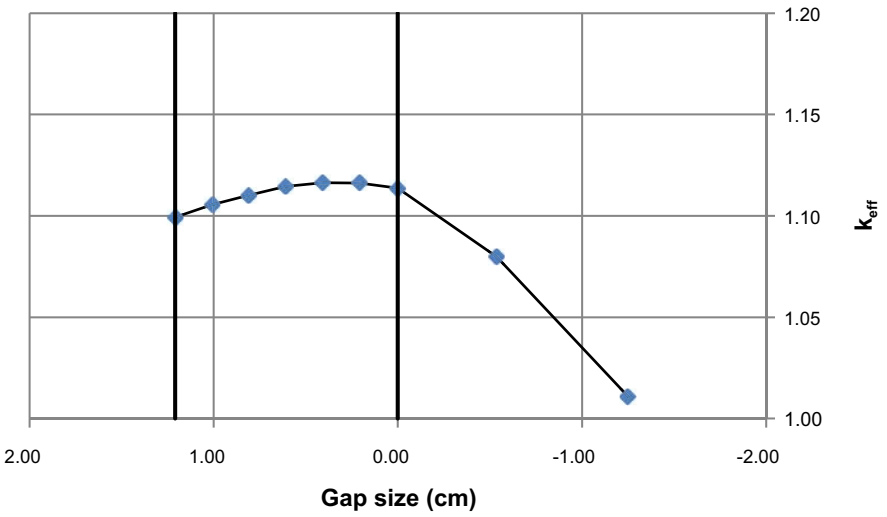

Figure 6-1. *Calculated k_{eff} vs gap size for a PWR canister. The growth of the magnetite layer into the assembly between the fuel rods has been represented with negative values for the gap size.*

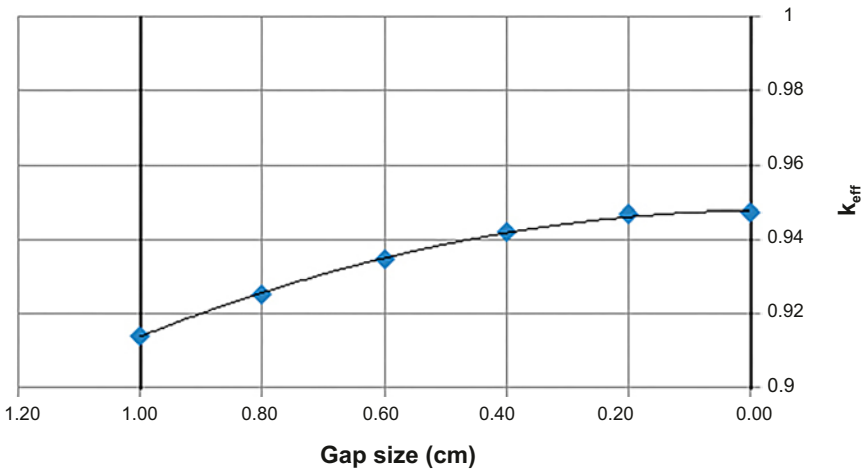

Figure 6-2. *Calculated k_{eff} vs gap size for a BWR canister.*

The carbon content of the cast iron insert is higher and it remains in the magnetite as graphite but, as it will be shown in the following sections, in these calculation cases there is magnetite between the fuel rods instead of water and the reactivity decreases considerably as compared to the case discussed here. A hypothetical calculation of the case with the gap between fuel channel and fuel rods filled with magnetite and 4 % carbon instead of 0.22 % resulted in a reactivity increase $\Delta k_{eff} = 0.0017$ for BWR and $\Delta k_{eff} = 0.0004$ for PWR. For this reason, we have not carried out calculations including 4 % graphite in the magnetite for the cases when there is magnetite between the fuel rods instead of water.

The geometry of the PWR and BWR cases with maximum reactivity is shown in Figure 6-3.

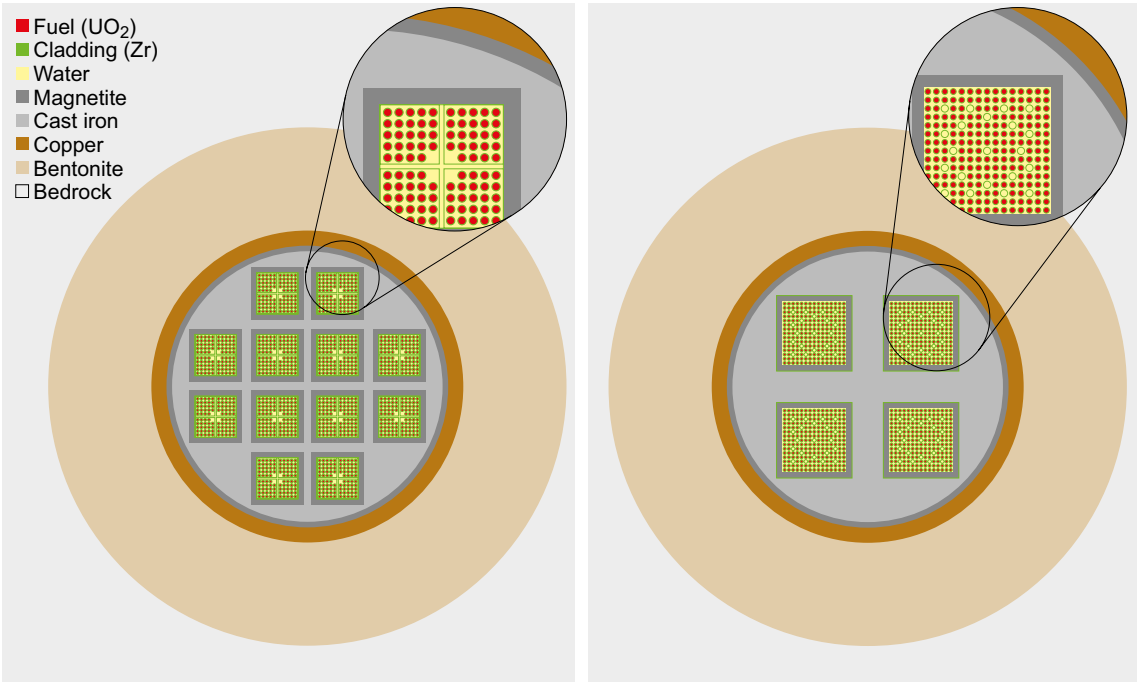

Figure 6-3. *Representation of the cross sections of the BWR and PWR inserts when the gap between the fuel rods (or fuel box) and the fuel channel wall is filled with magnetite. The area converted to magnetite in the fuel channels and in the copper-cast iron interface is represented, see magnification.*

One question is now how much water the hydrated magnetite will contain. A sensitivity study of the water content is done. The calculations are based on the cases above which give the highest k_{eff}, that is the magnetite layer is 1.9 cm in both the PWR and the BWR-case. Water is mixed in the magnetite layer according to Table 6-3 (see also Appendix A).

Table 6-3. Density of the hydrated magnetite with various water contents.

Water in the magnetite (weight %)	Density of hydrated magnetite (g/cm^3)	P-B of hydrated magnetite
0	5.17	2.10
5	4.26	2.68
10	3.65	3.57
20	2.82	4.81
30	2.30	6.75

The results are shown in Figure 6-4.

It can be seen that reactivity decreases when water is mixed into the magnetite, i.e. when hydrated magnetite with variable water content is formed as corrosion product instead of crystalline magnetite.

Another case with the magnetite layer replaced by water (in case Fe(II) ions are mainly sorbed or involved in clay transformations, as iron corrosion studies in the presence of clay indicate) was also analysed:

BWR: $k_{eff} = 0.8842$
PWR: $k_{eff} = 1.0635$

The conclusion is that the reactivity will be lower in this case as compared to the maximum reactivity case with magnetite filling the gap between channel wall and fuel.

Hydrogen is produced during the corrosion process. The effect of dissolved hydrogen in the water was investigated.

About 40 mM hydrogen could be dissolved in water at 50 bars pressure. Calculations show that this hydrogen concentration will increase the reactivity by $\Delta k_{eff} = 0.0006$ for PWR and $k_{eff} = 0.0009$ for BWR.

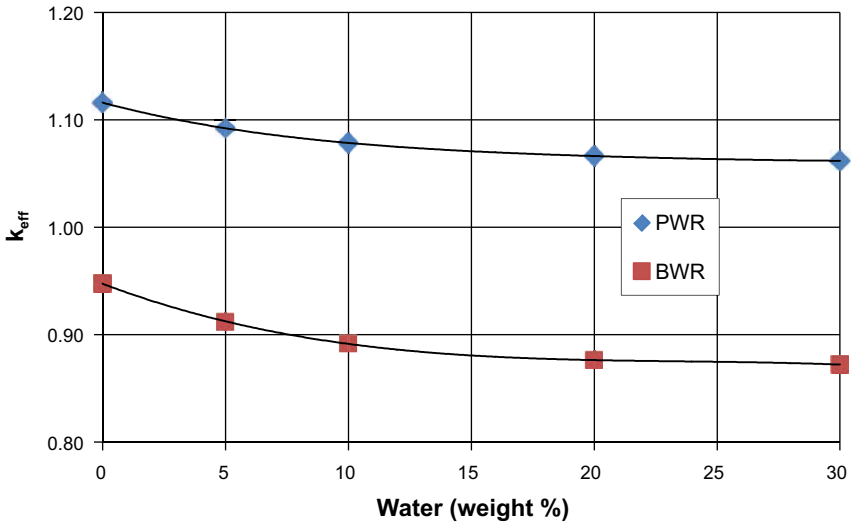

Figure 6-4. *k_{eff} as function of water content in the hydrated magnetite.*

6.4.2 Other corrosion products.

Besides from magnetite, siderite ($FeCO_3$) or mackinawite (FeS) could form in the canister. This is discussed in Section 6.3 and in Appendix B, where the formation of siderite + magnetite and mackinawite + magnetite is calculated separately for the PWR- and BWR case.

The calculation concerns the case when the corrosion layer almost touches the fuel rods for PWR and the fuel box wall in the BWR-case.

The results are shown in Table 6-4 for the PWR case and in Table 6-5 for the BWR case. It shows that a mixture between magnetite and siderite gives a slightly higher reactivity ($\Delta k = 0.0026$ for PWR and $\Delta k = 0.0037$ for BWR) compared with the case with pure magnetite.

Table 6-4. Calculated cases with mixtures of magnetite and siderite ($FeCO_3$), respectively mackinawite (FeS), for PWR.

Mixture	Density of mixture (g/cc)	P-B ratio	k_{eff}	Δk compared to main case
100 % Fe_3O_4 (main case)	5.17	2.1	1.1159	–
18 % Fe_3O_4 + 82 % $FeCO_3$	4.05	3.69	1.1185	0.0026
47 % Fe_3O_4 + 53 % $FeCO_3$	4.39	3.00	1.1176	0.0017
35 % Fe_3O_4 + 65 % FeS	4.57	2.52	1.1048	−0.0111
59 % Fe_3O_4 + 41 % FeS	4.78	2.36	1.1083	−0.0076

Table 6-5. Calculated cases with mixtures of magnetite and siderite ($FeCO_3$), respectively mackinawite (FeS), for BWR.

Mixture	Density of mixture (g/cc)	P-B ratio	k_{eff}	Δk compared to main case
100 % Fe_3O_4 (main case)	5.17	2.1	0.9475	–
52 % Fe_3O_4 + 48 % $FeCO_3$	4.45	2.77	0.9512	0.0037
35 % Fe_3O_4 + 65 % $FeCO_3$	4.62	2.66	0.9495	0.0019
32 % Fe_3O_4 + 68 % FeS	4.85	2.30	0.9395	−0.0081
25 % Fe_3O_4 + 75 % FeS	4.92	2.26	0.9407	−0.0069

6.4.3 Magnetite falls down into the fuel channel.

One uncertainty is if all the magnetite will stick to the channel wall or fall down into the channel. A case is analyzed assuming that the magnetite will fall into the fuel channel in a PWR canister. In this case it is assumed that the 1.9 cm magnetite layer will fall down at the bottom of the fuel channel into the fuel assembly. The result is that the space between fuel rods in the bottom part of the fuel assembly will be filled by magnetite and the top part will be surrounded by a larger water gap. The result is $k_{eff} \pm \sigma = 1.0656 \pm 0.0002$. This calculation is done with crystalline magnetite. The reduction of the reactivity is $\Delta k_{eff} = -0.0503$ compared to the maximum reactivity case, discussed in Section 6.4.1.

In the BWR case with boxed BWR fuel the box walls will prevent the magnetite to fall into the fuel assembly, so only the magnetite above the box will fall into the fuel assembly.

The result is $k_{eff} \pm \sigma = 0.8835 \pm 0.0002$. This calculation is also done with crystalline magnetite. The reduction of k_{eff} is $\Delta k_{eff} = -0.0640$ compared to the maximum reactivity base case in Section 6.4.1.

6.4.4 Magnetite layer grows resulting in reduced fuel rod pitch

In spite of the arguments presented for the mechanical properties of the hydrated magnetite, a calculation case where the expanding magnetite layer is assumed to be stiff and will instead press on the fuel assembly and push the fuel rods closer to each other. In these cases it is assumed that the pitch is reduced 0.3 mm both in the PWR case and the BWR case. The results are:

BWR: $k_{eff} = 0.9206$, a reduction of $\Delta k_{eff} = -0.0269$ compared to the maximum reactivity case in Section 6.4.1.

PWR: $k_{eff} = 1.0993$, a reduction of $\Delta k_{eff} = -0.0166$ compared to the maximum reactivity case in Section 6.4.1.

6.4.5 Magnetite flows into the fuel assembly

As discussed before, the internal geometrical surface is about 35 m^2 in BWR canister and about 17 m^2 for a PWR insert (SKB 2010c), while the free the volume in a BWR canister is about 1 m^3 and in a PWR canister about 0.7 m^3. The free space between fuel rods will be completely filled with crystalline magnetite in time intervals between 13 500 years for a BWR canister and 19 500 years in the case of a PWR insert for a corrosion rate of 1 µm/year. These time intervals will be shorter if more voluminous hydrated magnetite is formed. The assumption made here is that the mechanical properties of the hydrated magnetite are those described by Smart et al. (2006a), i.e. the growth of the magnetite layer will not cause the deformation of the fuel rods; instead the magnetite growing under pressure will be deformed and extrude in the space between fuel rods in a PWR canister. In this calculation the possibility for the magnetite formed in the space between cast iron and copper shell to extrude in the fuel channel through the large defect of a shear load scenario or through the insert lid in the corrosion scenario has been neglected: it would just shorten the time to reach at this situation. In the case of a BWR canister with boxed fuel, the fuel box is not considered to deform considerably, instead the hydrated magnetite produced by corrosion will be extruded into the fuel box when growing in a confined space. It is difficult to predict the properties of the corrosion layer for such large time spans, it may also convert to a more crystalline and compact solid with time either by itself or by interaction with ions in the groundwater, as shown by natural analogue studies.

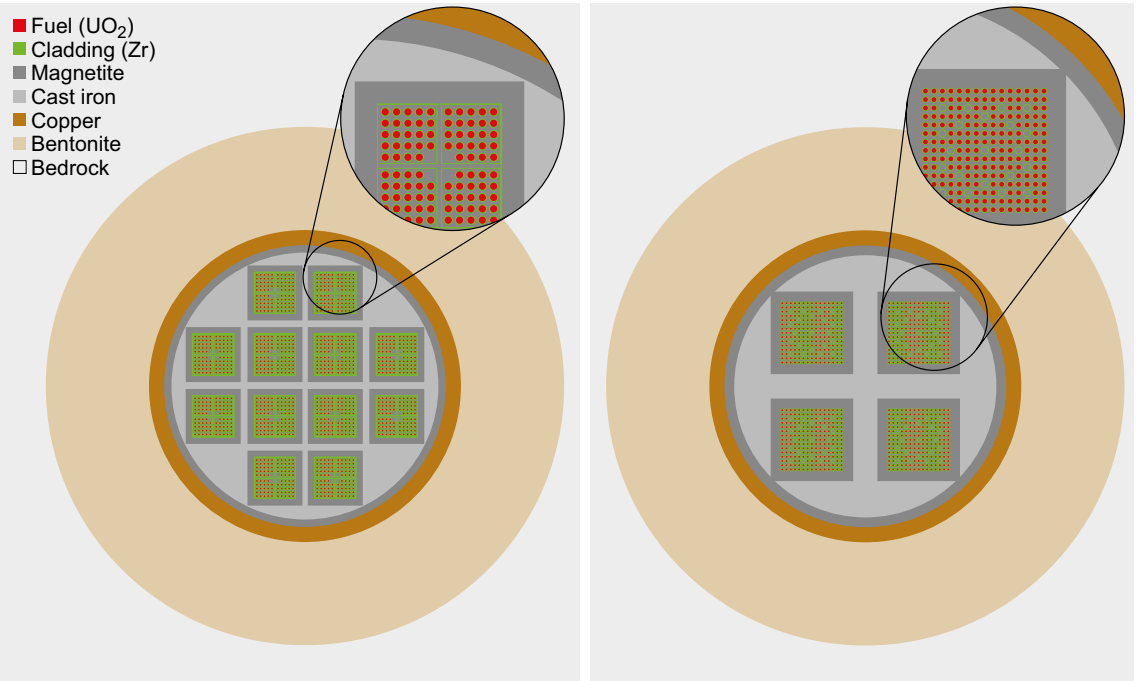

Figure 6-5. *Figure representing the canisters when the amount of corroded iron has produced enough magnetite to fill the space between the fuel rods and all the free space in the canister.*

However, as long as there is corroding metal, there will always be a relatively freshly formed outer corrosion layer, expected to have the properties observed during a few years of corrosion in the laboratory. A calculation case representing the situation with the whole free space of the canister filled with magnetite, hydrated at various degrees, has been carried out and is presented below.

For the scenario with corrosion process of the insert which continues, while the magnetite does not push the fuel rods together, but flows into and fills the space between fuel rods in the fuel assembly, the following cases were calculated:

The first case is that enough iron in the insert is corroded to produce magnetite that fills the space between fuel rods and all the free space in the canister. The results are:

BWR: $k_{eff} = 0.3009$
PWR: $k_{eff} = 0.3372$

Then four cases with hydrated magnetite with 5, 10, 20 and 30 % water are calculated.

The results are presented in Figure 6-6.

It can be seen that the reactivity in all these cases are well below the maximal reactivity cases in Section 6.4.1.

After all the free space in the canister has been filled with cast iron corrosion products, it seems difficult to envisage major changes in the geometry of the damaged canister, unless the copper shell is deformed. With a corrosion rate of 1 µm/year, the walls between fuel channels in a BWR canister are completely corroded in about 25 000 years, and the same holds for the thinner part of the cast iron insert between copper and fuel channels. In the PWR canister the part between fuel channels is thicker and the complete corrosion with the assumed corrosion rate occurs after about 62 000 years. The volume increase produced by the formation of new amounts of corrosion products after the free space in the canister is filled with magnetite will certainly cause some compaction of the corrosion product and its potential extrusion through the defect in the shear load scenario or the insert lid and the corroded Cu region where the bentonite clay has been eroded in the corrosion scenario. Alternatively, a deformation of the copper shell may be envisaged.

The cases when 5 cm of steel plus cast iron has corroded between the fuel channels in the BWR case and 13.5 cm in PWR case were calculated (see Figure 6-7). The same thickness of cast iron has corroded in the space between cast iron and copper. These cases are conservatively modelled assuming that the whole insert is corroded to crystalline magnetite (see Figure 6-8). The copper shell is not deformed in these cases. The results are:

BWR: $k_{eff} = 0.3178$
PWR: $k_{eff} = 0.3640$

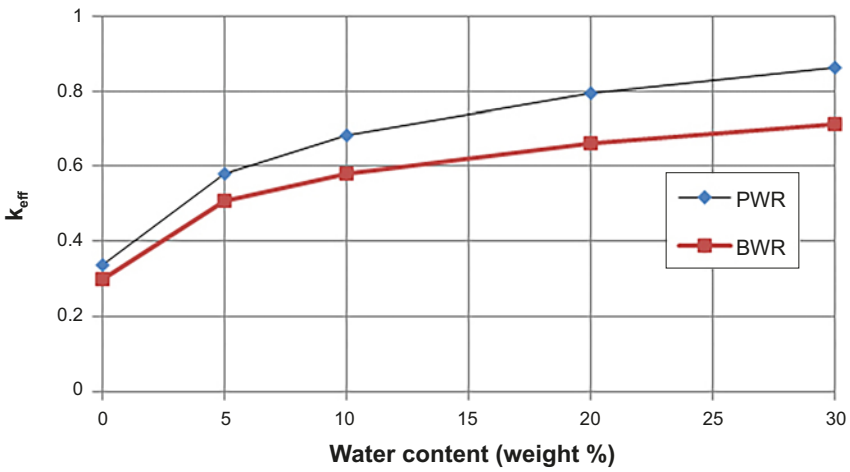

Figure 6-6. *Variation of k_{eff} when fuel channels and fuel assemblies are filled with magnetite, as a function of the water content in hydrated magnetite.*

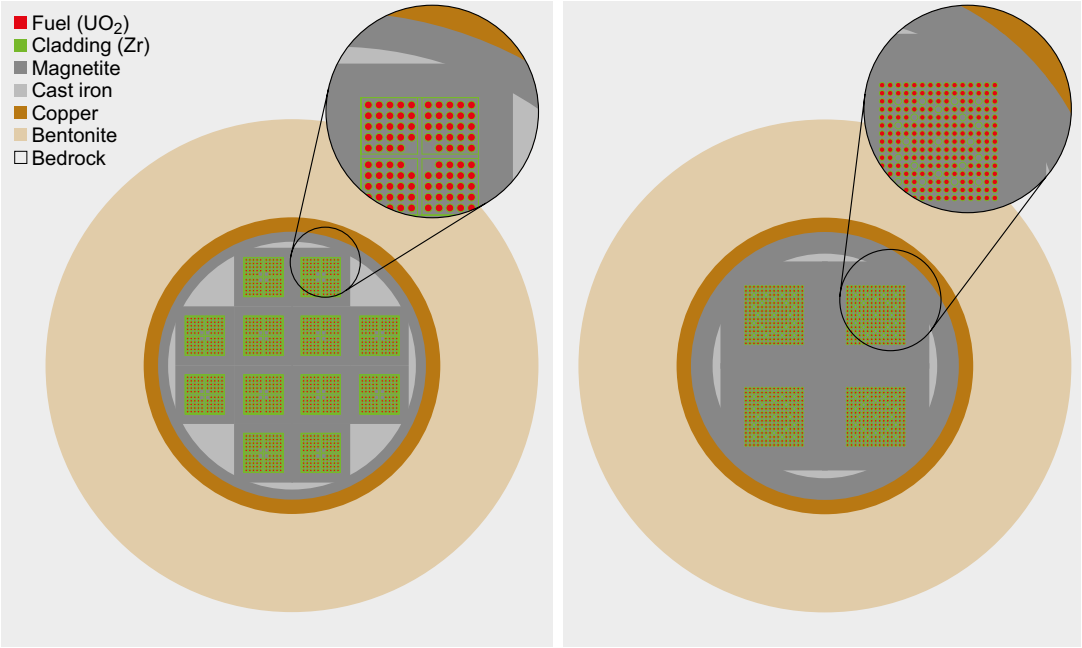

Figure 6-7. *Cross sections of BWR and PWR canisters when the carbon steel and cast iron between the fuel channels has corroded completely.*

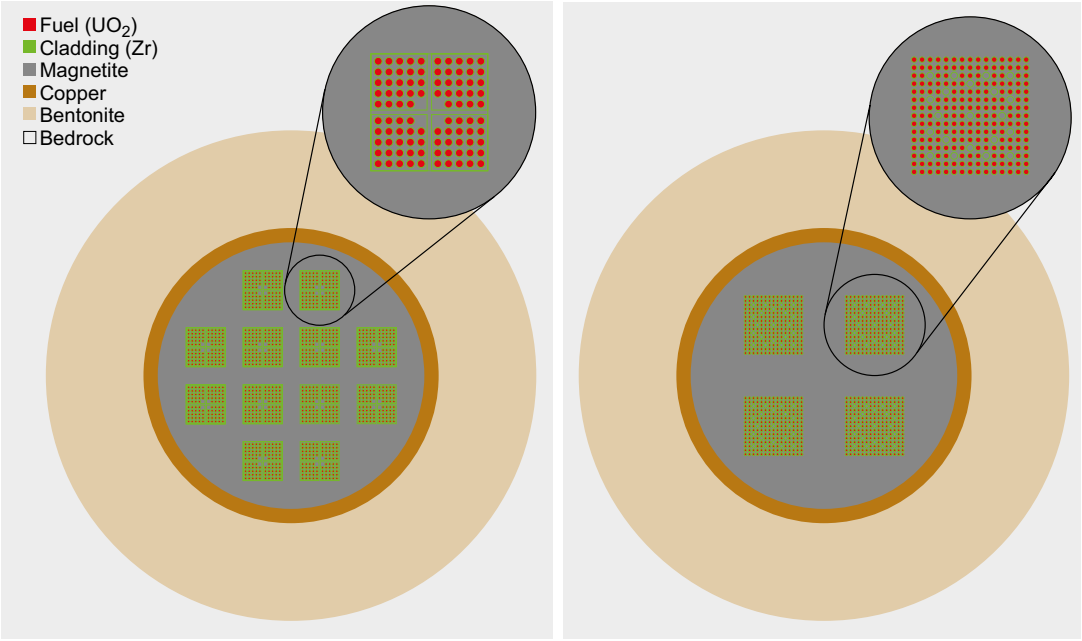

Figure 6-8. *The case when all the iron in the canister has been corroded and the canister is filled with magnetite is represented.*

The same cases were also calculated assuming that corrosion products will not flow out of the canister but instead stay within and expand the copper shell. The radius of insert is assumed to expand 10 cm and the copper shell is stretched out. The copper thickness is this reduced from 5 cm to 2.5 cm. The results are:

BWR: $k_{eff} = 0.3270$

PWR: $k_{eff} = 0.3725$

It can be seen that the reactivity will increase $\Delta k = 0.0092$ for BWR and $\Delta k = 0.0085$ for PWR compared to the case when the copper shell is not deformed.

One can present also the amount of magnetite pressed out in the large corrosion defect for the erosion/corrosion scenario or through the large defect in the earthquake scenario. In any case, the main difference with the previous case is that a larger part of the cast iron has been substituted by magnetite, but in both cases there is magnetite between the fuel rods.

6.4.6 Zirconium in the cladding and BWR fuel box converted to zirconium oxide

In spite of the arguments presented above that Zircaloy corrodes much more slowly than other materials, a calculation case has been carried out assuming that the Zircaloy corrodes faster.

In order to check the effect of the material changes during the fuel cladding corrosion, calculation cases with the two cm magnetite layer and all zirconium in the cladding converted to zirconium oxide have been carried out. The following cases were calculated.

In the PWR case, zirconium oxide replaces the cladding material, while the fuel column is intact, i.e. represents the moment at the end of the Zircaloy corrosion process, just before the pellets fall down. The result is $k_{eff} = 1.0928$.

For BWR case zirconium oxide replaces the cladding and box material and the fuel column is intact. The result is $k_{eff} = 0.9322$.

In both cases k_{eff} is lower than the main case. This depends on the fact that the volume increase during Zircaloy corrosion (P B-value for ZrO_2 is 1.56 (Shoesmith and Zagidulin 2011)) will reduce the water content in the fuel, resulting in lower reactivity.

6.4.7 Radial movement of fuel rods

The BWR assemblies contain part length rods, which are not attached to the assembly top plate. If the spacers are consumed by corrosion, the part length rods can move radially. The reactivity effect of moving part length rods was investigated for Svea 96 Optima 3. The rods were moved as far as possible inside the box and the central structure in the fuel assembly.

In the figures below the geometries for the different cases are shown. Note that all twelve fuel assemblies in a canister have the same changes in the positions of the part length rods.

a) Base case

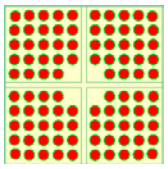

b) Part length rods in the corners moved out give a reactivity increase $\Delta k_{eff} = 0.0009$

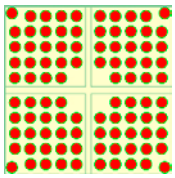

c) Part length rods in the corners moved in give a reactivity decrease $\Delta k_{eff} = -0.0025$

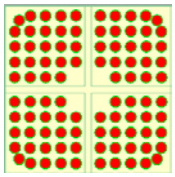

d) Part length rods in the center moved in give a reactivity increase $\Delta k_{eff} = 0.0034$

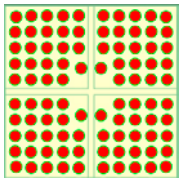

e) Part length rods in the center moved out give a reactivity decrease $\Delta k_{eff} = -0.0047$

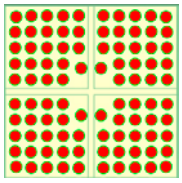

The results show that moving the part length rods in the center inwards can result in a reactivity increase in this case by $\Delta k_{eff} = 0.0034$.

Some BWR assembly types have no top plate. In this case all fuel rods at the top of the fuel assembly can move radially. The following cases with displaced fuel rods in the upper part of the assembly have been analyzed.

f) Fuel rods moved outwards in top of the assembly, pitch increased from 1.2768 cm to 1.318 cm. This gives a reactivity increase $\Delta k_{eff} = 0.0004$.

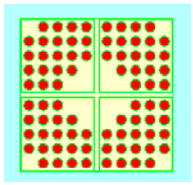

g) Fuel rods moved outwards in top of the assembly, pitch increased from 1.2768 cm to 1.318 cm and fuel rods moved creating water holes in the assembly. This gives a reactivity increase $\Delta k_{eff} = 0.0011$.

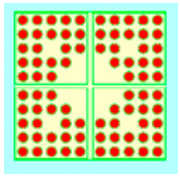

h) Fuel rods moved outwards in top of the assembly, pitch increased from 1.2768 cm to 1.318 cm and the fuel rods moved to create even more water holes in the assembly. This gives a reactivity increase $\Delta k_{eff} = 0.0031$.

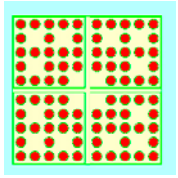

6.4.8 Fuel pellets fall at the bottom of the fuel channel

In this calculation case, it is assumed that all the fuel cladding is oxidized to ZrO_2. The oxidized cladding is assumed to disintegrate and together with the fuel pellets fall down in the fuel channels at the bottom of the canister, most likely as fuel fragments (i.e. each pellet produces several fragments).

The geometry of a pile of fragments at the bottom of the channel is difficult to model. It is therefore assumed that pellets are intact and the number of pellets is the same as in the fuel assembly. The pellets will most likely fall down and end up in a random geometry. As this is not possible to model, the calculations were done assuming the pellets are organized in a larger number of shorter columns in different square patterns with different heights of the pellet pile, thus changing the ratio of UO_2 and water, see Table 6-6.

Table 6-6. Fuel rod patterns.

Fuel type	Fuel rod pattern	Height of pellet pile (cm)	UO_2/water
BWR	10 × 10-4 (96 rods)	369.0	0.56
	10 × 10	354.2	0.61
	11 × 11	292.8	0.96
	12 × 12	246.0	1.72
PWR	15 × 15-21 (204 rods)	365.8	0.55
	15 × 15	331.7	0.66
	16 × 16	291.5	0.86
	17 × 17	258.2	1.17

In the nominal case the volume UO_2 is 20.1 dm^3 in a BWR fuel element and the free water volume (channel volume minus the volumes of the structural parts and UO_2) in the fuel channel is 35.8 dm^3, hence the UO_2/water ratio is 0.56.

For nominal PWR case the UO_2 volume is 50.6 dm^3, the free water volume is 92.7 dm^3 and the UO_2/water ratio is 0.55.

The results are shown in Figure 6-9. When pellets fall down, the UO_2/water ratio increases (more UO_2 per volume water) as compared to the initial state of the fuel element. In fact, the first point of each curve in Figure 6-9 represents the UO_2/water ratio for the initial geometry of the fuel element.

In the diagram in Figure 6-9 it can be seen that increased UO_2/water ratio results in decreased reactivity. A pile of fuel fragments (which are of smaller and variable size as compared to the pellets) is expected to have higher UO_2/water ratio (Brouwers 2006), thus lower reactivity.

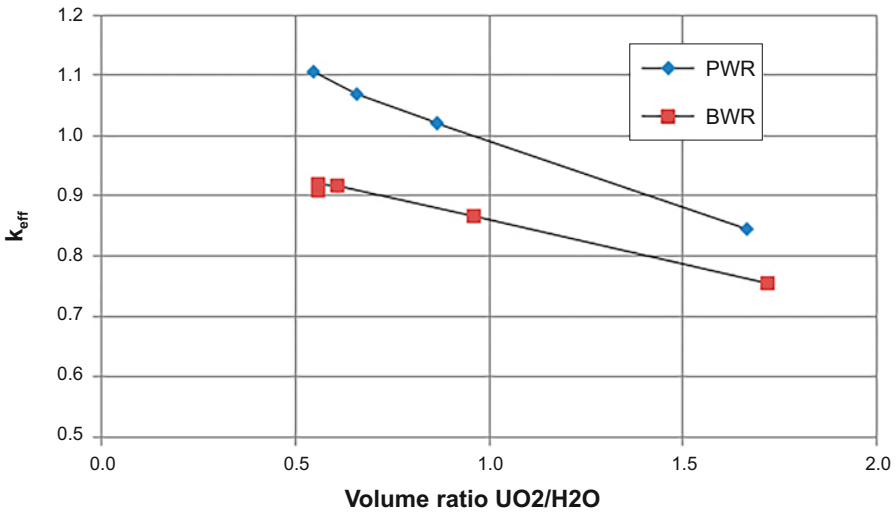

Figure 6-9. *k_{eff} as function of UO_2/water ratio.*

The same geometries were calculated assuming that the spaces in and around the fuel assemblies are filled with magnetite. Two qualities of magnetite was used, one with crystalline magnetite and one with magnetite containing 30 % water. The results are shown in Table 6-7.

Table 6-7. Results with magnetite in the fuel and fuel channels.

Fuel type	Fuel rod pattern	Height of pellet pile (cm)	Crystalline magnetite in fuel, k_{eff}	Magnetite with 30 % water in fuel, k_{eff}
BWR	10 × 10-4 (96 rods)	369	0.3351	0.7075
	10 × 10	354.2	0.3241	0.7232
	11 × 11	292.8	0.3572	0.7463
	12 × 12	246	0.3774	0.7528
PWR	15 × 15-21 (204 rods)	365.8	0.3738	0.8049
	15 × 15	331.7	0.3857	0.8000
	16 × 16	291.5	0.4056	0.7936
	18 × 18	230.3	0.4442	0.7576

Fuel rods containing burnable absorber (BA-rods) are subject to lower power output during reactor operation because Gd-oxide causes a decrease of the thermal conductivity and of the melting point of the doped fuel (IAEA 1995). For this reason, the oxidation of their cladding from outside due to water corrosion is expected to be lower, due to the lower surface temperature as compared to the other fuel rods. The same holds for the inside oxidation due to excess oxygen produced by fissions, hence their cladding should in general be less oxidized than this of the other fuel rods during reactor operation. Since the material composition of the cladding of all fuel rods in a fuel element is the same, while the thickness of the un-corroded material is expected to be slightly larger for the BA-rods, calculation cases with preferential corrosion of the cladding of burnable absorber rods and their deposition as pellets or fragments at the bottom of fuel channels have not been carried out.

A variation of this case is the scenario in which one or several fuel rods have completely corroded cladding, hence their fuel pellets are as a pile at the bottom of the fuel channel, while the other fuel rods have only partially corroded cladding and have the initial vertical positions. This case has been analysed elsewhere[9], assuming also a removal of the cladding and of the fuel box, as well as a maximum pin pitch expansion (see next paragraph). In all cases with rods which have their pellets at the bottom of the fuel channel, a decrease in reactivity as compared to the value obtained for the complete set of rods in their vertical position is observed. For this reason, it has not been analyzed further here.

There are two cases which cause a reactivity increase discussed in Ranta-aho (2012)[10], which we have not considered for the reasons discussed briefly below. The first one concerns corrosion of Zircaloy with complete disappearance of Zr from the metal layer, instead of its conversion to ZrO_2(s), as considered in our case. In fact, there is some transport of Zr out of the canister with the water flow through the deposition hole which can cause a decrease of the thickness of the oxide layer. Given the low solubility of ZrO_2(s) in near neutral pH (Brown et al. 2005, Baes and Mesmer 1976), even with a relatively high water flow of 300 liter/year, about 3×10^{-5} mol Zr/year are transported out of the canister. This would cause a decrease of the ZrO_2(s) layer thickness by 6×10^{-2} nm/year for a BWR canister with a total Zircaloy surface of 10.95 m^2 and by 2×10^{-2} nm for a PWR canister with a total Zr surface of 31.4 m^2. Both these decreases are negligible as compared to the oxide layer thickness increase due to metal corrosion (1.56 nm/year for the lowest metal corrosion rate considered here of 1 nm/year). Because the calculations show that it is not possible for the oxide to be physically removed from the canister, this case was not considered further here.

[9, 10] Ranta-aho A, 2012. Criticality safety analysis of BWR, PWR and VVER-440 disposal canisters in the final disposal facility, TVO Memorandum 144244, internal TVO document.

The second case concerns a symmetric (uniform) expansion of the fuel pin lattice which causes reactivity increase. This is considered to happen when the top and bottom plates, as well as the grid spacers, have been corroded, i.e. after several thousands of years. The corrosion of all metals in the canister produces corrosion products which have a higher molar volume than the metal, i.e. the free space in the canister is expected to decrease and not increase. In Section 6.4.2 we present arguments that the free space in the canister is filled with magnetite after the corrosion of about 13 mm carbon steel in a BWR canister, which is expected to occur faster than the corrosion of an equivalent thickness of stainless steel in the top and bottom plates. Further corrosion of the remaining cast iron will produce new amounts of magnetite, causing its compaction inside the canister and extrusion of the surplus magnetite through the damaged part of the canister. The same arguments presented for the transport out of Zr are valid also for the anoxic corrosion products of iron: their solubility is higher than that of ZrO_2, still the amounts produced each year are much larger and the thickness decrease due to transport of Fe ions out of the canister with water flow is negligible. The copper shell is expected to have a much longer lifetime than cast iron and stainless steel and will anyhow confine the fuel rods and the corrosion products of the insert. For this reasons, we have not considered the expansion of the fuel pin lattice as a possible alternative of the canister evolution.

6.4.9 Corrosion of UO_2

It is assumed that the fuel cladding is no barrier to water and the corrosion of the fuel pellets will start when water enters in the breached canister. Corrosion of the UO_2 in the pellets results in that some uranium is released as U(VI) from the fuel and is afterwards reduced and precipitated as UO_2(s) on the corrosion layer of cast iron.

In order to carry out calculations in this case, spent fuel with a burnup 34 MWd/kgU was considered and not fresh fuel as in all the other of cases. In this calculation model the fuel material is irradiated and its heavy metal composition is 2.6 % U-235, 0.9 % Pu, 96 % U-238, with the remainder being other actinides and fission products. In the Pu case, the content of Pu-239 is 70 %.

Further, it was assumed that 18 kg of fuel material is uniformly distributed on the inner surface of the magnetite layer. This assumption would be valid when the corrosion of cast iron proceeds with 0.1 μm/year; hence more fuel material is released as compared to the shorter time to reach this configuration with a corrosion rate of 1 μm/year. The fuel pellet diameter has been reduced corresponding to the lost amount of fuel material. These effects result in increases of the reactivity:

PWR: $\Delta k_{eff} = 0.0019$

BWR: $\Delta k_{eff} = 0.0026$

In the next case other actinides and fission products are removed from the layer on the surface of the magnetite, the remaining material will be 2.6 % U-235, 0.9 % Pu, 96.5 % U-238. The reactivity increase is calculated to:

PWR: $\Delta k_{eff} = 0.0032$

BWR: $\Delta k_{eff} = 0.0037$

In both cases the reactivity will increase compared to the max reactivity case in Section 6.4.1. The case with only U and Pu gives the highest reactivity increase.

As discussed in Section 6.3.4, any selective release of burnable absorber (Gd) during the oxidative dissolution of spent fuel is not expected. The lanthanide metals have very low oxygen potentials (Kleykamp 1985), hence they are homogenously distributed in the UO_2 fuel matrix (Imoto 1986, Kleykamp 1988). Further, since they are as Ln(III) ions in the matrix and cannot be oxidized at a higher state (as e.g. U(IV)), they are even expected to be left behind in the matrix by certain authors (Hanson and Stout 2004). In any case, a congruent release of the lanthanide fission products such as Gd is assumed in the SKB's fuel dissolution model.

6.4.10 Less probable scenarios and calculation cases

Redistribution of fuel rods after an earthquake was analysed. The displacement of the upper half of the sheared canister is moved diagonally about 1 cm and the upper sheared fuel rods fall in the lower part of the canister into the gap between the fuel assembly and the channel wall, see Figure 6-10.

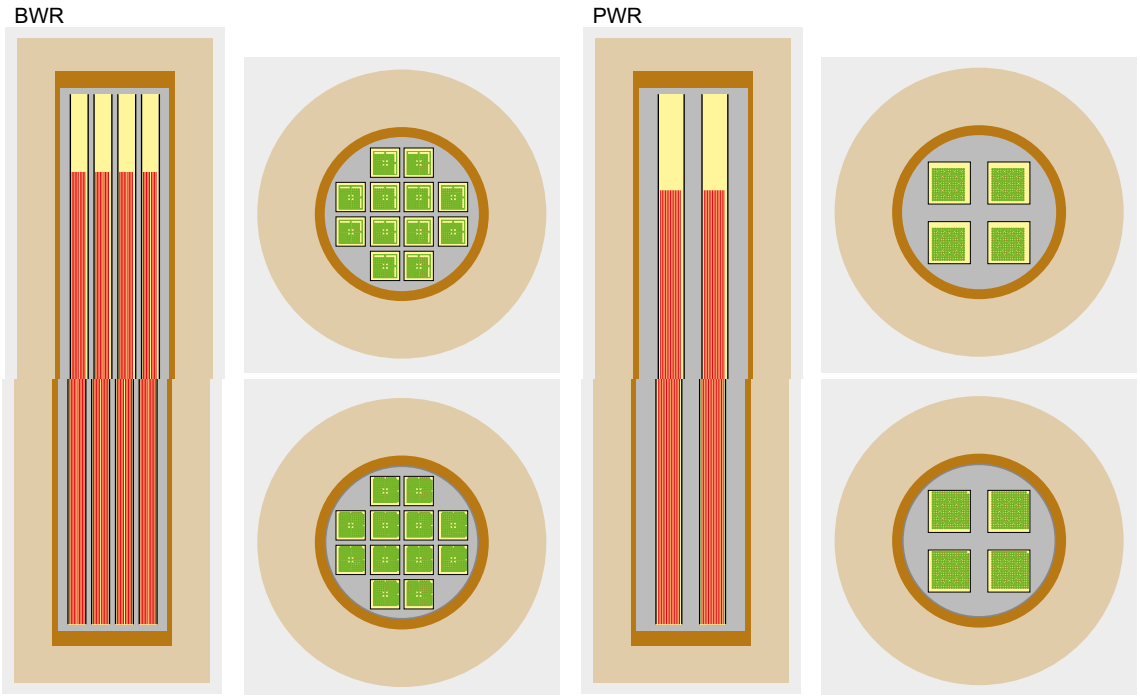

Figure 6-10. *Earthquake case for a BWR or a BWR canister.*

In this case it is assumed that the canister geometry is intact, that is corrosion has not started. The results are:

BWR k_{eff} = 0.9968
PWR k_{eff} = 1.1305

This case is hypothetical, because the canister would withstand a 1 cm displacement. To realise it, a larger displacement should take place first, then in some way a back movement brings the cut fuel rods at exactly 1 cm displacement from the initial position. Given the extremely low probability of such an event, this case was considered to be a residual risk and therefore not considered as basis for the final analysis of the reactivity increase.

6.5 Analysis

The reactivity development is summarized in Table 6-8 for PWR and BWR respectively. The cases are assigned numbers in order to facilitate the analysis and comparison between the different cases.

In Table 6-8 k_{eff} for the different cases are shown for BWR and PWR. The reactivity differences between the cases and the base case (case 2) are also shown. A positive reactivity difference indicates that the burn up requirement has to be increased compared to values given in criticality analysis for the KBS-3 system and final repository of spent nuclear fuel[11].

The k_{eff} will increase during the magnetite formation and closing of the water gap between the fuel and channel walls. When the gap is closed (case 3 in Table 6-8) the k_{eff} has increased by $\Delta k = 0.0166$ for the PWR case and $\Delta k = 0.0333$ for the BWR case, as compared to the base case (case 2 in Table 6-8).

Formation of hydrated magnetite with various amounts of water contributes to a decrease of the reactivity in the damaged canister, cases 4 to 7.

[11] Johansson F, Kirkegaard J, Johansson A, 2014. Kriticitetsanalys för KBS-3 systemet och slutförvaring av använt bränsle. SKBdoc 1422106, internal SKB document.

Table 6-8. Summary of the calculated cases.

Case no	Description	BWR		PWR	
		k_{eff}	Δk compared to base case	k_{eff}	Δk compared to base case
1	Dry canister	0.2322		0.2900	
2	Base case, water filled	0.9142		1.0993	
3	Magnetite in gap 5.17 g/cc	0.9475	0.0333	1.1159	0.0166
4	Hydrated magnetite in gap – 5 % water	0.9119	−0.0023	1.0921	−0.0072
5	Hydrated magnetite in gap – 10 % water	0.8918	−0.0224	1.0784	−0.0209
6	Hydrated magnetite in gap – 20 % water	0.8761	−0.0381	1.0602	−0.0391
7	Hydrated magnetite in gap – 30 % water	0.8721	−0.0421	1.0618	−0.0375
8	Magnetite replaced by water	0.8842	−0.0300	1.0635	−0.0358
9	$FeCO_3$ + Fe_3O_4 in gap	0.9512	0.0370	1.1185	0.0192
10	FeS + Fe_3O_4 in gap	0.9407	0.0265	1.1083	0.0090
11	Magnetite layer (5.17 g/cc) falls down into fuel	0.8835	−0.0307	1.0656	−0.0337
12	Reduced rod pitch gap closed	0.9206	0.0064	1.0993	0.0000
13	Magnetite flows into fuel 5.17 g/cc	0.3009	−0.6133	0.3372	−0.7621
14	Hydrated magnetite (5 % water) flows into fuel	0.5090	−0.4052	0.5791	−0.5202
15	Hydrated magnetite (10 % water) flows into fuel	0.5798	−0.3344	0.6818	−0.4175
16	Hydrated magnetite (20 % water) flows into fuel	0.6610	−0.2532	0.7340	−0.3653
17	Hydrated magnetite (30 % water) flows into fuel	0.7139	−0.2003	0.8603	−0.2390
18	The whole insert is corroded	0.3178	−0.5964	0.3640	−0.7353
19	Magnetite 5.17 g/cc, Zr oxidized fuel column intact	0.9322	0.0180	1.0928	−0.0065
20	Pellets fall down in channels	0.9204	0.0062	1.1069	0.0076
21	Earthquake case	0.9968	0.0826	1.1305	0.0312

In addition, a calculation case simulating sorption and reaction of Fe(II) ions produced by the corrosion with the nearby bentonite clay (observed during iron corrosion experiments in the presence of clay) assuming water at the place of the corroded iron layer has been carried out (case 8). The resulting k_{eff} is lower than in the case with the highest reactivity (case 3).

Assuming other corrosion products will be produced, it can be seen that $FeCO_3$ (siderite, case 9) will increase the reactivity as compared to case 3. The reason for that is the carbon content in siderite.

The case when the formed magnetite falls down at the bottom of the fuel channel (case 11) contributes in a decrease of the reactivity as compared to case 3.

If the expanding magnetite layer is assumed to be stiff and will press on the fuel assembly, the internal water gaps in the fuel assembly will close and the fuel rod center to center spacing will decrease (case 12). In this case the reactivity will decrease compared to case 3.

The cases 13 to18 when the magnetite will flow into the fuel assemblies will result in reactivity much lower than in case 3.

If it is assumed that Zircaloy corrodes relatively quickly (case 19) and zirconium oxide replaces the cladding material during time intervals when only the gap between cast iron and fuel rods is filled with magnetite, the reactivity will decrease as compared to case 3 if the fuel column is still intact, just before the pellets fall down.

Starting from case 19, the oxidized cladding is assumed to disintegrate and together with the fuel pellets fall down between the fuel rods in the fuel channels to the bottom of the canister (case 20), most likely as fuel fragments (i.e. each pellet produces several fragments). This will result in a reactivity decrease compared to case 3.

The corrosion of UO_2 fuel can result in that fuel material is released from the fuel and is precipitated on the corrosion layer of cast iron. The isotopic composition of the fuel material corresponds to a burnup of 34 MWd/kgU. This resulting increase in reactivity is calculated to:

PWR: $\Delta k_{eff} = 0.0032$

BWR: $\Delta k_{eff} = 0.0037$

From Table 6-8, cases 2 and 3, and the discussion above, it can be concluded that reactivity increases when the corrosion products fill the water gap between the fuel assembly and the channel wall. If the corrosion products consist of a mixture of magnetite with siderite, the worst case is achieved (case 9 in Table 6-8). Additional reactivity increases occur if hydrogen will be dissolved in the water and if corrosion of fuel material results in that fuel material is precipitated on the corrosion layer of cast iron.

7 Summary and conclusions

Assuming that disposal canisters are water filled, the oxidation of the cast iron insert will generate corrosion products. These have lower density than iron so the water gap between the fuel and the fuel channels will close. If the corrosion product is magnetite this effect will increase the reactivity with $\Delta k_{eff} = 0.0333$ for BWR and $\Delta k_{eff} = 0.0166$ for PWR compared to the base case (case 2). Assuming that siderite is produced besides from magnetite, the reactivity will increase further; $\Delta k_{eff} = 0.0026$ for PWR and $\Delta k_{eff} = 0.0037$ for BWR. Also assuming the hydrogen will be dissolved in the groundwater, an additional reactivity increase will occur, $\Delta k_{eff} = 0.0006$ for PWR and $\Delta k_{eff} = 0.0009$ for BWR (for a concentration of 40 mM dissolved hydrogen). Corrosion of the fuel can result in the release of oxidized U and Pu species, which are afterwards reduced and precipitated on the corroded iron layer. This will give additional reactivity increase, for PWR $\Delta k_{eff} = 0.0032$ and for BWR $\Delta k_{eff} = 0.0037$. Radial movements of the fuel rods that are not attached to the top plate in BWR assemblies could give an additional reactivity increase, $\Delta k_{eff} = 0.0034$. If carbon is included in the magnetite composition the reactivity increases $\Delta k_{eff} = 0.0004$ the BWR case, while in the PWR case the increase was negligible. Finally the statistical uncertainties in Keno are included for both cases. The reactivity effects are summarized in table 7-1.

Table 7-1. Summary of reactivity effects.

Effect	Reactivity increase Δk	
	BWR	PWR
Gap closed by magnetite	0.0333	0.0166
Magnetite + siderite in gap	0.0037	0.0026
H_2 dissolved in water	0.0009	0.0006
U and Pu on the inner iron surface	0.0037	0.0032
Radial movement of fuel rods	0.0034	–
Carbon content in channel walls	0.0004	0
Combination of Keno statistical uncertainties	0.0007	0.0007
Sum	0.0461	0.0237

In summary the total reactivity increase will add up to $\Delta k_{eff} = 0.0237$ for PWR and $\Delta k_{eff} = 0.0461$ for BWR compared to the nominal case. This corresponds to an increase in the burnup credit requirement of approximately 5 MWd/kg U for PWR and 8 MWd/kgU for BWR.

References

SKB's (Svensk Kärnbränslehantering AB) publications can be found at www.skb.com/publications.

ACI, 2007. ACI manual of concrete inspection. 10th ed. Detroit: American Concrete Institute.

Agrenius L, 2010. Criticality safety calculations of disposal canisters, SKBdoc 1193244 ver 3.0, Svensk Kärnbränslehantering AB.

Andra, 2005. Dossier Argile – The phenomenological evolution of a geological repository. Châtenay-Malabry: Agence nationale pour la gestion des déchets radioactifs (Andra).

Baes C F, Mesmer R E, 1976. The hydrolysis of cations. New York: Wiley.

Blackwood D J, Naish C C, Sharland S M, Thompson A M, 2002. Experimental and modelling study to assess the initiation of crevice corrosion in stainless steel containers for radioactive waste. Report AEAT/ERRA-0300, AEA Technology, UK.

Bond A E, Hoch A R, Jones G D, Tomczyk A J, Wiggin R M, Worraker W J, 1997. Assessment of a spent fuel disposal canister. Assessment studies for a copper canister with cast steel inner component. SKB TR 97-19, Svensk Kärnbränslehantering AB.

Brouwers H J H, 2006. Particle size distribution and packing fraction of geometric random packings. Physical Review E 74, 031309. doi:10.1103/PhysRevE.74.031309

Brown P, Curti E, Grambow B, Ekberg C, 2005. Chemical thermodynamics. Vol. 8, Chemical thermodynamics of Zirconium. Amsterdam: Elsevier.

Cui D, Spahiu K, 2002. The reduction of U(VI) on corroded iron under anoxic groundwater conditions. Radiochimica Acta 90, 623–628.

de Combarieu G, Barboux P, Minet Y, 2007. Iron corrosion in Callovo-Oxfordian argilite : From experiments to thermodynamic/kinetic modelling. Physics and Chemistry of the Earth, Parts A/B/C 32, 346–358.

Dinh H T, Kuever J, Mußmann M, Hassel A W, Stratmann M, Widdel F, 2004. Iron corrosion by novel anaerobic microorganisms. Nature 427, 829–832.

Enning D, Garrelfs J, 2014. Corrosion of iron by sulphate-reducing bacteria: new views on an old problem. Applied and Environmental Microbiology 80, 1226–1236.

Enning D, Venzlaff H, Garrelfs J, Dinh H T, Meyer V, Stratmann M, Widdel F, 2012. Marine sulfate-reducing bacteria cause serious corrosion of iron under electroconductive biogenic mineral crust. Environmental Microbiology 14, 1772–1787.

Farrel J, Bostick W D, Jarabek R J, Fiedor J N, 1999. Uranium removal from ground water using zero valent iron media. Ground Water 37, 618–624.

Féron D, Crusset D, Gras J-M, 2009. Corrosion issues in the French high-level nuclear waste programme. Corrosion 65, 213–223.

Fiedor J N, Bostick W D, Jarabek R, Farrell J, 1998. Understanding the mechanism of uranium removal from groundwater by zero valent iron using x-ray photoelectron spectoscopy, Environmental Science & Technology 32, 1466–1473.

Grambow B, Smailos E, Geckeis H, Müller R, Hentschel H, 1996. Sorption and reduction of uranium(VI) on iron corrosion products under reducing saline conditions. Radiochimica Acta 74, 149–154.

Gras J-M, 2014. State of the art of ^{14}C in Zircaloy and Zr alloys-^{14}C release from zirconium alloy hulls. Deliverable 3.1 of the EU-Project Cast. European Commission.

Gribi P, Johnson L, Sutter D, Smith P, Post, Snellmann M, 2008. Safety assessment for KBS-3H repository at Olkiluoto. Process report. SKB R-08-36, Svensk Kärnbränslehantering AB.

Gu B, Liang L, Dickey J, Dai S, 1998. Reductive precipitation of uranium(VI) by zero-valent iron. Journal of Environmental Science & Technology 32, 3366–3373.

Hanson B D, Stout R B, 2004. Re-examining the dissolution of spent fuel: a comparison of different methods for calculating rates. In Hanchar J M, Stroes-Gascoyne S, Browning L (eds). Scientific Basis for Nuclear Waste Management XXVIII: symposium held in San Francisco, California, USA, 13–16 April 2004. Warrendale, PA: Materials Research Society. (Materials Research Society Symposium Proceedings 824), 89–94.

Haynes W M, Lide D R, Bruno T J (eds), 2012. CRC handbook of chemistry and physics: a ready-reference book of chemical and physical data. 93rd ed. Boca Raton, FL: CRC Press.

IAEA, 1995. Characteristics and use of urania-gadolinia fuels. IAEA-TECDOC-844, International Atomic Energy Agency.

IAEA, 1998. Durability of spent nuclear fuels and facility components in wet storage. IAEA-TECDOC-1012, International Atomic Energy Agency.

Imoto S, 1986. Chemical state of fission products in irradiated UO_2. Journal of Nuclear Materials 140, 19–27.

Johnson A B, Burke S P, 1996. K-basin corrosion report. WHC-EP-087, Westinghouse Hanford Company, Richland, Washington.

Johnson A B, Francis B, 1980. Durability of metals from archaeological objects, metal meteorites and native metals. PNL-3198, Battelle Pacific Northwest Laboratory, Richland, Washington.

Joyce S, Woollard A, Marsic N, Sidborn M, 2015. Future evolution of groundwater composition at Forsmark during an extended temperate period. SKB R-14-26, Svensk Kärnbränslehantering AB.

Kienzler B, Gmal B, 2007. Critical safe disposal of spent fuel: the behaviour of neutron poisons. In Proceedings of the International Conference on GLOBAL 2007, Boise, Idaho, 9–13 September 2007, 1453–1460.

King F, 2008. Corrosion of carbon steel under anaerobic conditions in a repository for SF and HLW in Opalinus Clay. Nagra Technical Report 08-12, Nagra, Switzerland.

King F, 2014. Durability of high level waste and spent fuel disposal canisters-an overview of the combined effect of chemical and mechanical degradation mechanisms, Appendix B2: Corrosion of carbon steel and Appendix B3: Corrosion of cast iron. RWMD Report 17697/TR/03, Radioactive Waste Management Directorate, UK.

Kleykamp H, 1985. The chemical state of the fission products in oxide fuels. Journal of Nuclear Materials 131, 221–246.

Kleykamp H, 1988. The chemical state of fission products in oxide fuels at different stages of the nuclear fuel cycle. Nuclear Technology 80, 412–422.

Kotz J, Treichel P, Townsend J, 2008. Chemistry and chemical reactivity. Vol. 2. Boston: Cenage Learning.

Kursten B, Smailos E, Azkarate I, Werme L, Smart N R, Marx G, Cuñado M A, Santarini G, 2004. COBECOMA. State-of-the-art document on the COrrosion BEhaviour of COntainer Materials. Final report. CONTRACT N° FIKW-CT-20014-20138. European Commission.

Lee C T, Qin Z, Odziemkowski M, Shoesmith D W, 2006. The influence of groundwater anions on the impedance behaviour of carbon steel corroding under anoxic conditions. Electrochimica Acta 51, 1558–1568.

Legrand L, Savoye S, Chausse A, Messina R, 2000. Study of oxidation products formed on iron in solutions containing bicarbonate/carbonate. Electrochimica Acta 46, 111–117.

Mineralogy database, 2012. Magnetite mineral data. Available at: http://webmineral.com/data/Magnetite.shtml#.V853S7VA8Xk

Navrotsky A, Mazeina L, Majzlan J, 2008. Size-driven structural and thermodynamic complexity in iron oxides. Science 329, 1635–1638.

Neff D, Dillman P, Descostes, M, Beranger G, 2006. Corrosion of iron archaeological artefacts in soil: estimation of average corrosion rates and thermodynamic calculations. Corrosion Science 48, 2947–2970.

Odziemkowski M S, Schumacher T T, Gillham R W, Reardon E J, 1998. Mechanism of oxide film formation on iron in simulating groundwater solutions: Raman spectroscopic studies. Corrosion Science 40, 371–389.

Pilling N B, Bedworth R E, 1923. The oxidation of metals at high temperature. Journal of the Institute of Metals 29, 529–591.

Refait P, Bourdoiseau J A, Jeannin M, Nguyen D D, Romaine A, Sabot R, 2012. Electrochemical formation of carbonarted corrosion products on carbon steel in deaerated solutions. Electrochimica Acta 79, 210–217.

Saheb M, Neff D, Dillmann P, Matthiessen H, Foy E, 2008. Long term corrosion behaviour of low-carbon steel in anoxic environment: characterization of archaeological artefacts. Journal of Nuclear Materials 379, 118–123.

Saheb M, Descostes M, Neff D, Mathiesen H, Michelin A, Dillmann P, 2010. Iron corrosion in anoxic soil: comparison between thermodynamic modelling and ferrous artefacts characterized along with in situ geochemical conditions. Applied Geochemistry 25, 1937–1948.

Saheb M, Berger P, Raimbault L, Neff D, Dillmann P, 2012. Investigation of iron long term corrosion mechanism in anoxic media using deuterium tracing. Journal of Nuclear Materials 423, 61–66.

Salas J, Gimeno M J, Auqué L, Molinero J, Gómez J, Juárez I, 2010. SR-Site –hydrogeochemical evolution of the Forsmark site. SKB TR-10-58, Svensk Kärnbränslehantering AB.

Savoye S, Legrand L, Sagon G, Lecomte S, Chausse A, Messina R, Toulhoat P, 2001. Experimental investigations on iron corrosion products formed in bicarbonate/carbonate containing solutions at 90 °C. Corrosion Science 43, 2049–2064.

SCALE, 2006. SCALE: A modular code system for performing standardized computer analyses for licensing evaluations, ORNL/TM-2005/39, Version 5.1, Vols. I–III, November 2006, Oak Ridge National Laboratory, Oak Ridge, Tennessee. Available from Radiation Safety Information Computational Center at Oak Ridge National Laboratory as CCC-732.

Shoesmith D W, Zagidulin D, 2010. The corrosion of zirconium under deep geologic repository conditions. Journal of Nuclear Materials 418, 292–306.

Shoesmith D W, Taylor P, Bayley M G, Owen D G, 1980. The formation of ferrous monosulfide polymorfs during the corrosion of iron by aqueous hydrogen sulphide at 21 °C. Journal of Electrochemical Society 127, 1007–1015.

SKB, 2010a. Fuel and canister process report for the safety assessment SR-Site. SKB TR-10-46, Svensk Kärnbränslehantering AB.

SKB, 2010b. Data report for the safety assessment SR-Site. SKB TR-10-52, Svensk Kärnbränslehantering AB.

SKB, 2010c. Design, production and initial state of the canister. SKB TR-10-14, Svensk Kärnbränslehantering AB.

SKB, 2011. Long-term safety for the final repository for spent nuclear fuel at Forsmark. Main report for the SR-Site project. SKB TR-11-01, Svensk Kärnbränslehantering AB.

Smart N R, Adams R, 2006. Natural analogues for expansion due to the anaerobic corrosion of ferrous materials. SKB TR-06-44, Svensk Kärnbränslehantering AB.

Smart N R, Bond A E, Crossley J A, Lovegrove P C and Werme L, 2001. Mechanical properties of oxides formed by anaerobic corrosion of steel. In Hart K P, Lumpkin G R (eds). Scientific basis for nuclear waste management XXIV: symposium held in Sydney, Australia, 27–31 August 2000. Warrendale, PA: Materials Research Society. (Materials Research Society Symposium Proceedings 663), 477–485.

Smart N R, Blackwood D J, Werme L, 2002a. Anaerobic corrosion of carbon steel and cast iron in artificial groundwaters: Part 1 – Electrochemical aspects. Corrosion 58, 547–559.

Smart N R, Blackwood D J, Werme L, 2002b. Anaerobic corrosion of carbon steel and cast iron in artificial groundwaters: Part 2 – Gas generation. Corrosion 58, 627–637.

Smart N R, Rance A P and Werme L O, 2004a. Anaerobic corrosion of steel in bentonite. In Oversby V M, Werme L O (eds). Scientific basis for nuclear waste management XXVII: symposium held in Kalmar, Sweden, 15–19 June 2003. Warrendale, PA: Materials Research Society. (Materials Research Society Symposium Proceedings 807), 441–446.

Smart N R, Blackwood D J, Marsh G P, Naish C C, O'Brien T M, Rance A P, Thomas M I, 2004b. The anaerobic corrosion of carbon and stainless steels in simulated cementitious environments: A summary review of Nirex research. Report AEAT/ERRA-0313, AEA Technology, UK.

Smart N R, Rance A P, Fennell P A, 2006a. Expansion due to the anaerobic corrosion of iron. SKB TR-06-41, Svensk Kärnbränslehantering AB.

Smart N R, Rance A P, Carlson L, Werme L O, 2006b. Further studies of the anaerobic corrosion of steel in bentonite. In Van Iseghem P (ed). Scientific basis for nuclear waste management XXIX: proceedings of a meeting held in Ghent, Belgium, 12–16 September 2005. Warrendale, PA: Materials Research Society. (Materials Research Society Symposium Proceedings 932), 813–820.

Smart N R, Bate F, Carlson L, Cave M R, Green K, Heath T G, Hoch A R, Hunter F M, Karnland O, Kemp S J, Milodowski A E, Olsson S, Pritchard A M, Rance A P, Shaw R A, Taylor H, Vickers B, Werme L, Williams C L, 2008. Interactions between iron corrosion products and bentonite. Deliverable 2.3.9 of EU-Project NF-PRO. European Commission.

Swanton S W, Baston G M N, Smart N R, 2015. Rates of steel corrosion and carbon-14 release from irradiated steels – state of the art review. Deliverable 2.1of the EU-project CAST. European Commission.

Tweedle D, 1992. The Anglian helmet from 16-22 Coppergate. London: York Archaeological Trust by the Council for British Archaeology.

Wada R, Nishimura T, Fujiwara K, Tanabe M, Mihara M, 1999. Experimental study on hydrogen gas generation rate from corrosion of Zircaloy and stainless steel under anaerobic alkaline conditions. In Proceedings of the Seventh International Conference on Radioactive Waste Management and Environmental Remediation ICEM '99, Nagoya, Japan, 26–30 September 1999.

Winsley R J, 2008. Modelling investigation of a defective copper canister as the steel shell corrodes. Task one, technical note to summarise literature review on mechanical properties of oxides. NWMO TR-2008-SA32, Nuclear Waste Management Organization, Canada.

Appendix A

Properties of hydrated magnetite

The hydrated magnetite contains different proportions of water in the structure. This kind of mixtures can be calculated with water content in weight % or in volume %. The first alternative is discussed, i.e. weight percent.

a) Magnetite with 5 % weight water: the density is 4, 26 g/cm^3, for a molecular formula of $Fe_3O_4 \cdot 0.68H_2O$, the molar weight is 243.72, the Pilling-Bedworth ratio is 2.68 (see next case for details of the calculation).

b) A sample of magnetite that contains 10 % weight water is made up of 90 g magnetite and 10 g water. The volume of 90 g magnetite is 90/5, 17g/cm^3 = 17.41 cm^3, while that of 10 g water is 10 cm^3. The total volume is 17.41 + 10 = 27.41 cm^3, while the total weight is 100 g. The density of this mixture is 3.65 g/cm^3. The calculation of the P-B ratio needs the calculation of molar weight.

We have 90/231.53 = 0.3887 mol magnetite and 10/18 = 0.556 mol water, i.e. 1 mol magnetite contains 2.573 mol water and can be written $Fe_3O_4 \cdot 2.573\ H_2O$ with molar weight 277.88. With these values we have:

$$R_{PB} = \frac{V_{oxide}}{V_{metal}} = \frac{M_{oxide} \cdot \rho_{metal}}{n \cdot M_{metal} \cdot \rho_{oxide}} = \frac{277.88 \cdot 7.85}{3 \cdot 55.845 \cdot 3.65} = 3.57$$

It already produces a large volume increase compared to crystalline magnetite and for this reason we have not assumed hydrated magnetite containing higher than 30 percent water.

c For hydrated magnetite with 20 % water, we have: 80/5.17 = 15.47 cm^3 the volume of magnetite and 20 cm^3 water, resulting in a density of 100/35.47 cm^3 = 2.82 g/cm^3. For 80/231.53 = 0.3455 mol magnetite and 1.11 mol water, or $Fe_3O_4 \cdot 3.216H_2O$ with molecular weight 289.42 g/mol, the P-B ratio is 4.81.

d) For 30 percent water, we have 70/5.17 = 13.54 cm^3 magnetite volume and 30 cm^3 water, giving a density of 100/43.54 = 2.297 g/cm^3. For 70/231.53 = 0.302 mol magnetite and 1.667 mol water, or $Fe_3O_4 \cdot 5.52\ H_2O$ with molecular weight 330.89, the P-B ratio results 6.75. Such high P-B ratio would fill the canister quite quickly.

Initially we assumed this water ratio as the highest possible, based on the hydration number of the iron ion in water, i.e. $Fe(H_2O)_6$. A literature search on the subject suggests that the amount of water in the hydrated magnetite is lower than that, even though no direct measurements for hydrated magnetite could be found. In the literature, reference is made to $Fe_3O_4 \cdot 0.5H_2O$ as hydrated green magnetite or $Fe_3O_4 \cdot H_2O$ (Kotz et al. 2008). These water contents would correspond to 3.74 % respectively 7.2 % in weight of water. In the preparation of heavy concrete with hydrated magnetite as inert material (ACI 2007), the densities of such a material are reported in the range 4.2–4.8 gcm^{-3}. These densities for hydrated magnetite correspond approximately to magnetite with 5.54 % respectively 1.85 % in weight of water. The same source (ACI 2007) reports water contents of 12–18 % for hydrated Fe(III) oxides such as goethite and limonite, known to contain much more water than hydrated magnetite (Navrotsky et al. 2008).

Appendix B

Calculation of mixed corrosion product layers

The total amount of iron corroded per year with a corrosion rate 1 μm/year is different for a PWR canister (17 m^2 surface) and a BWR canister (35 m^2 surface). For 35 m^2 about 35 cm^3 iron corrodes per year (or 274.75 g or 4.92 mol Fe), while for 17 m^2 surface 17 cm^3 iron corrode per year (or 133.45 g iron or 2.39 mol Fe). Below the formation of siderite + magnetite and mackinawite + magnetite mixtures is calculated separately for the PWR and BWR case.

1. **PWR canister.** The total internal surface area is 17 m^2, meaning that 17 cm^3 iron corrode per year with a corrosion rate of 1 μm/year. This corresponds to 133.45 g iron or 2.39 moles of iron. In case the corrosion product is magnetite, 184.4 g magnetite is produced.
   a) The first assumption is that out of the 2.39 mol Fe which corrodes per year, 1.8 mol Fe ($1.8 \times 55.845 = 100.52$ g) give 208.54 g siderite as corrosion product, while 0.59 mol Fe (32.95 g) give 45.53 g magnetite. In total 254.07 gram mixture are produced by the corrosion of 133.45 g Fe and they have a volume (for crystalline products) 208.54/3.87 = 53.89 cm^3 for siderite and 45.53/5.17 = 8.8 cm^3 for magnetite. The total volume for the mixture is 62.7 cm^3, i.e. the average density for the mixture is 4.05 g/cm^3. The weight percent of siderite in the mixture (siderite + magnetite) is 208.54/254.07 = 82.08 % siderite while the rest is magnetite. The simplest volume increase is calculated by the volume of Fe(s) (17 cm^3) and the volume of corrosion products which is 62.7 cm^3, i.e. $R_{P\text{-}B} = 62.7/17 = 3.69$.
   b) Another alternative, probably more possible to happen in reality, is that the 1.8 moles of iron (100.52 g) give 1.8 moles of $FeCO_3$(s) corresponding to 208.54 g siderite, while the corrosion with magnetite formation continues with 1 μm/year all the time, i.e. the amount in gram of iron corroded this way is 133.45 g, giving 184.4 g magnetite. In total 392.94 g mixture siderite + magnetite is produced per year, with 53.07 weight percent siderite (208.54/392.94). The volumes of the corrosion products for crystalline solids are 53.89 cm^3 for siderite and 35.67 cm^3 for magnetite, in total 89.56 cm^3. The density of the mixture is 392.94 g/89.56 cm^3 = 4.39 g/cm^3. The volume increase is calculated from (100.52+133.45)/7.85 = 29.8 cm^3 Fe metal has given 89.56 cm^3 mixture siderite + magnetite, i.e. $R_{P\text{-}B} = 89.56/29.8 = 3.0$.
   c) In the case of mackinawite formation, according to the first assumption, out of the 2.39 mol Fe corroded, 1.5 mol ($1.5 \times 55.845 = 83.77$ g) give 127.05 g mackinawite and 0.89 mol Fe (49.7 g) give 68.69 g magnetite. The total weight of corrosion products is 195.71 g while total volume 127.02/4.3 = 29.54 cm^3 mackinawite plus 13.29 cm^3 magnetite = 42.83 cm^3. The weight percent of mackinawite in the corrosion products is 127.02/195.71 = 65 % The average density of the corrosion product mixture is 195.71/42.83 = 4.57 g/cm^3. This gives a volume increase or P-B ratio of 42.83/17 = 2.52 for the case of crystalline products.
   d) The alternative case here would be that 1.5 moles of sulphide as FeS are formed independently of the magnetite, which is formed with 1 μm/ year (i.e. about 2.39 moles iron corroded per year to give magnetite). In case c) it was assumed that 2.29 moles Fe corrodes in total and out of this total amount, 1.5 moles corrode to give sulphide. In case d) the assumption is that since there is enough water, corrosion to give magnetite continues as usual and on top of this amount, 1.5 moles Fe corrode to give sulphide. The amount of sulphide is constrained by mass balance arguments.

In this case, 83.77 g iron corrode to give 127.05 g mackinawite each year, while 133.45 g iron corrode to give 184.4 g magnetite. In total 311.45 g mixture mackinawite + magnetite are formed, where mackinawite is 127.05/311.45 = 40.8 % in weight. The total volume of the mixture is 127.05/4.3 = 29.55 cm^3 mackinawite plus 184.4/5.17 = 35.67 cm^3 magnetite = 65.22 cm^3. The average density of the corrosion product mixture is 311.45/65.22 = 4.77 g/cm^3, and since 27.67 cm^3 iron is converted to 65.22 cm^3 mixture, the P-B ratio is thus 2.36.

The corrosion layer is calculated from the iron corroded (cm) times $R_{P\text{-}B}$ of the mixture.

Below are the two tables calculated for the corrosion layer filling the gap between the fuel rod surface (or fuel box surface for BWR) and fuel channel wall:

Table B-1. Data for case a) and c) of the mixed corrosion layer filling the gap.

Material	Density (g/cm^3)	RP-B	Corroded Fe (cm)	Corrosion layer (cm)
Fe_3O_4 100 %	5.17	2.1	0.9	1.9
$FeCO_3$ 82 % + Fe_3O_4 18 %	4.05	3.69	0.37	1.37
FeS 65 % + Fe_3O_4 35 %	4.57	2.52	0.66	1.66

Table B-2. Data for case b) and d) of the mixed corrosion layer filling the gap.

Material	Density (g/cm^3)	R_{P-B}	Corroded Fe (cm)	Corrosion layer(cm)
Fe_3O_4 100 %	5.17	2.1	0.9	1.9
$FeCO_3$ 53 % + Fe_3O_4 47 %	4.39	3.0	0.5	1.5
FeS 26 % + Fe_3O_4 74 %	4.77	2.36	0.735	1.735

2. **BWR canister.** The total surface area is 35 m^2, meaning that with a corrosion rate of 1 μm/year, 35 cm^3 iron (or 274.75 g iron or 4.92 mol iron) is corroded each year and in case only magnetite is formed, 379.7 g magnetite is produced each year.
   e) The assumption in the first case is that out of the 4.92 mol Fe which corrodes per year, 1.8 mol Fe (1.8 × 55.845 = 100.52 g) give 208.54 g siderite as corrosion product while the rest, 3.12 mol Fe (172.24 g) give 222.07 g magnetite. In total 430.61 gram mixture are produced by the corrosion of 274.75 g Fe and they have a volume (for crystalline products) 208.54/3.87 = 53.89 cm^3 for siderite and 222.07/5.17 = 42.95 cm^3 for magnetite. The total volume for the mixture is 96.84 cm^3, i.e. average density for the mixture is 4.45 g/cm^3. The weight percent of siderite in the mixture siderite + magnetite is 208.54/430.61 = 48.4 % siderite and the rest is magnetite. The simplest volume increase is calculated by the volume of Fe(s) (35 cm^3) and the volume of corrosion products is 96.84 cm^3, i.e. R P-B = 96.84/35 = 2.77.
   f) The other alternative, probably more possible to happen in reality, is that the 1.8 moles of iron (100.52 g) give 1.8 moles of $FeCO_3$(s) corresponding to 208.54 g siderite, while the corrosion with magnetite formation continues with 1 μm/year all the time, i.e. the amount in gram of iron corroded this way is 274.75 g, giving 379.7 g magnetite. In total 588.24 g mixture siderite + magnetite is produced per year, with 35.4 weight percent siderite (208.54/588.24). The volumes of the corrosion products for crystalline solids are 53.89 cm^3 for siderite and 73.44 cm^3 for magnetite, in total 127.33 cm^3. The density of the mixture is 588.24 g/127.33 cm^3 = 4.62 g/cm^3. The volume increase is calculated from (100.52+274.75)/7.85 = 47.8 cm^3 Fe metal has given 127.33 cm^3 mixture siderite + magnetite, i.e. R_{P-B} = 2.66.
   g) In the case of mackinawite formation, according to the first assumption, out of the 4.92 mol Fe corroded, 1.5 mol (1.5 × 55.845 = 83.77 g) give 127.05 g mackinawite and 3.42 mol Fe (191 g) give 263.94 g magnetite. The total weight of corrosion products is 391 g while the total volume is 127.02/4.3 = 29.54 cm^3 mackinawite plus 51.05 cm^3 magnetite = 80.59 cm^3. The weight percent of mackinawite in the corrosion products is 127.05/391 = 32.5 %. The average density of the corrosion product mixture is 391/80.59 = 4.85 g/cm^3. This gives a volume increase or P-B ratio of 80.59/35 = 2.30 for the case of crystalline products.
   h) The alternative case here would be that 1.5 moles of sulphide as FeS are formed independently of the magnetite, which is formed with 1 μm/ year (i.e. about 4.92 moles iron corroded per year to give magnetite). In this case the assumption is that since there is enough water, corrosion to give magnetite continues as usual and on top of this amount, 1.5 moles Fe corrode to give sulphide.

In this case, 83.77 g iron corrodes to give 127.05 g mackinawite each year, while 274.75 g iron corrode to give 379.7 g magnetite. In total, 506.75 g mixture of mackinawite + magnetite is formed, where mackinawite is 127.05/506.75 = 25.07 % in weight. The volume of the corrosion product mixture is 127.05/4.3 = 29.55 cm^3 mackinawite and 379.7/5.17 = 73.44 cm^3 magnetite, in total 103 cm^3 mixture. The average density of the corrosion product mixture is 506.75/103 = 4.92 g/cm^3, and since 45.67 cm^3 iron is converted to 103 cm^3 mixture, the P-B ratio is thus 2.26.

Below are both tables calculated for a corrosion layer which fills completely the gap.

Table B-3. Data for case e) and g) of the mixed corrosion layer which fills the gap.

Material	Density (g/cm^3)	R_{P-B}	Corroded Fe (cm)	Corrosion layer(cm)
Fe_3O_4 100 %	5.17	2.1	0.9	1.9
$FeCO_3$ 48 % + Fe_3O_4 52 %	4.45	2.77	0.565	1.565
FeS 32.5 % + Fe_3O_4 67.5 %	4.57	2.30	0.77	1.77

Table B-4. Data for case f) and h) of the mixed corrosion layer which fills the gap.

Material	Density (g/cm^3)	R_{P-B}	Corroded Fe (cm)	Corrosion layer(cm)
Fe_3O_4 100 %	5.17	2.1	0.9	1.9
$FeCO_3$ 53 % + Fe_3O_4 47 %	4.62	2.66	0.60	1.60
FeS 25 % + Fe_3O_4 75 %	4.92	2.26	0.79	1.79

Arkitektkopia AB, Bromma, 2016

SKB is tasked with managing Swedish nuclear and radioactive waste in a safe way.

skb.se